Cation-selective Mutations in the M2 Domain of the Inhibitory Glycine Receptor Channel Reveal Determinants of Ion-Charge Selectivity

Angelo Keramidas,[1] Andrew J. Moorhouse,[1] Kerrie D. Pierce,[2] Peter R. Schofield,[2] and Peter H. Barry[1]

[1]Department of Physiology and Pharmacology, University of New South Wales, Sydney 2052, Australia
[2]The Garvan Institute of Medical Research, Darlinghurst, Sydney 2010, Australia

ABSTRACT Ligand-gated ion channel receptors mediate neuronal inhibition or excitation depending on their ion charge selectivity. An investigation into the determinants of ion charge selectivity of the anion-selective α1 homomeric glycine receptor (α1 glycine receptor [GlyR]) was undertaken using point mutations to residues lining the extra- and intracellular ends of the ion channel. Five mutant GlyRs were studied. A single substitution at the intracellular mouth of the channel (A-1′E GlyR) was sufficient to convert the channels to select cations over anions with $P_{Cl}/P_{Na} = 0.34$. This result delimits the selectivity filter and provides evidence that electrostatic interactions between permeating ions and pore residues are a critical factor in ion charge selectivity. The P-2′Δ mutant GlyR retained its anion selectivity ($P_{Cl}/P_{Na} = 3.81$), but it was much reduced compared with the wild-type (WT) GlyR ($P_{Cl}/P_{Na} = 27.9$). When the A-1′E and the P-2′Δ mutations were combined (selectivity double mutant [SDM] GlyR), the relative cation permeability was enhanced ($P_{Cl}/P_{Na} = 0.13$). The SDM GlyR was also Ca^{2+} permeable ($P_{Ca}/P_{Na} = 0.29$). Neutralizing the extracellular mouth of the SDM GlyR ion channel (SDM+R19′A GlyR) produced a more Ca^{2+}-permeable channel ($P_{Ca}/P_{Na} = 0.73$), without drastically altering monovalent charge selectivity ($P_{Cl}/P_{Na} = 0.23$). The SDM+R19′E GlyR, which introduces a negatively charged ring at the extracellular mouth of the channel, further enhanced Ca^{2+} permeability ($P_{Ca}/P_{Na} = 0.92$), with little effect on monovalent selectivity ($P_{Cl}/P_{Na} = 0.19$). Estimates of the minimum pore diameter of the A-1′E, SDM, SDM+R19′A, and SDM+R19′E GlyRs revealed that these pores are larger than the α1 GlyR, with the SDM-based GlyRs being comparable in diameter to the cation-selective nicotinic acetylcholine receptors. This result provides evidence that the diameter of the ion channel is also an important factor in ion charge selectivity.

KEY WORDS: ligand-gated ion channels • electrostatics • pore diameter • permeability • selectivity filter

INTRODUCTION

Selectivity is a fundamental biophysical property of ion channels. The majority of ion channels identified to-date have distinct ion selectivities, including the members of the nicotinic acetylcholine receptor type family of ligand-gated ion channels (LGICs).* These receptor channels mediate hyperpolarizing (inhibitory) or depolarizing (excitatory) synaptic potentials by virtue of the opening of their ion-selective channels in response to a neurotransmitter. The members of this family include the anion-selective glycine receptor (GlyR) and γ-aminobutyric acid receptors ($GABA_AR$, $GABA_CR$) and the cation-selective nicotinic acetylcholine receptor (nAChR) and 5-hydroxytryptamine-type 3 receptor ($5\text{-}HT_3R$). All the members of this LGIC family are pentameric and structurally homologous (Noda et al., 1983; Schofield et al., 1987; Grenningloh et al., 1987; Langosch et al., 1988; Maricq et al., 1991). Each of their five receptor subunits is composed of a large extracellular domain, which binds agonists and antagonists, and four transmembrane domains (M1-M4). Various investigative techniques, including chemical labeling and site-directed mutagenesis (for reviews see Lester, 1992; Karlin and Akabas, 1995), have provided evidence that the five M2 transmembrane domains demarcate the ion channel.

LGICs generally have rings of charge associated with their channels. For example, α and β subunits comprising the anion-selective GlyRs, $GABA_ARs$, and the ρ1 subunit of $GABA_CRs$ have positively charged arginine residues at the intracellular channel mouth at position 0' (Fig. 1). By contrast, the subunits of the cation-selective $5\text{-}HT_{3A}Rs$ and nAChRs invariably have a positively charged lysine residue (or arginine in $5\text{-}HT_{3A}Rs$), which is generally preceded by a negatively charged glutamate (the nAChR γ and ε subunits have a glutamine residue in the equivalent position). It has been demonstrated that the negatively charged glu-

Address correspondence to Peter H. Barry, Department of Physiology and Pharmacology, University of New South Wales, Sydney 2052, Australia. Tel.: (61) 2-9385-1101; Fax: (61) 2-9385-1099; E-mail: p.barry@unsw.edu.au

*Abbreviations used in this paper: $5\text{-}HT_3R$, 5-hydroxytryptamine-type 3 receptor; GABAR, γ-aminobutyric acid receptor; GlyR, glycine receptor; LGIC, ligand-gated ion channel; nAChR, nicotinic acetylcholine receptor; SDM, selectivity double mutant; STM, selectivity triple mutant; WT, wild-type.

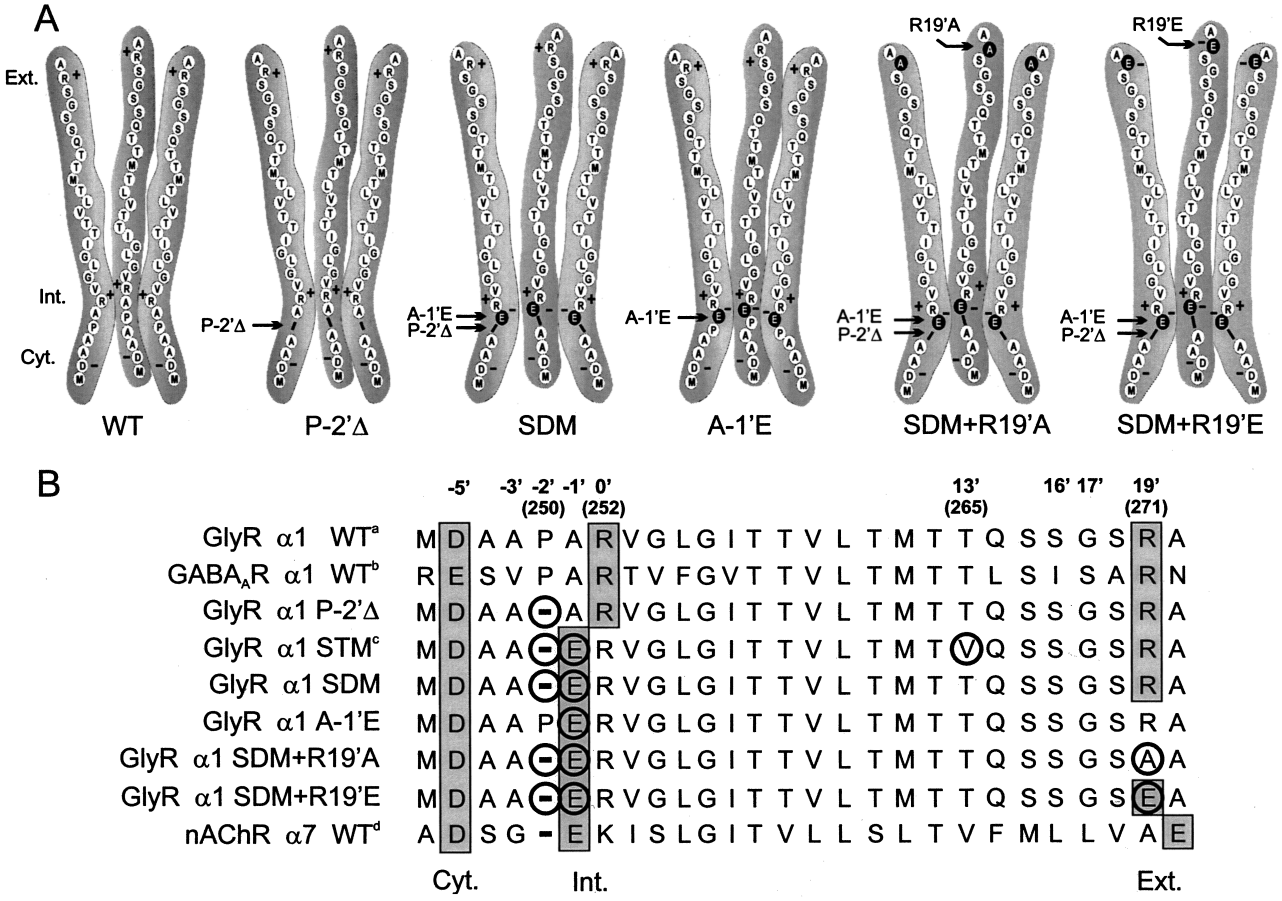

FIGURE 1. Schematic representations of M2 domains. (A) Schematic diagrams showing three M2 domains of, from left to right, WT, P-2'Δ, SDM, A-1'E, SDM+R19'A, and SDM+R19'E GlyRs. Single amino acids are drawn as circles with their single letter code. The mutated residues are shown in black and indicated by arrows. The rings of charge within the permeant ion pathway are denoted as Ext. (extracellular), Int. (intermediate), and Cyt. (cytoplasmic). (B) Selected M2 sequences for the GlyR homomeric channels investigated in this study together with the anion-selective GABA$_A$R α1 WT and the cation-selective nAChR α7 WT and GlyR α1 STM mutant. The rings of charged residues believed to predominate in ion permeation are shown in shaded boxes and indicated by Ext., Int., and Cyt. as above, with the generalized LGIC numbering for M2 domains (e.g., Lester, 1992) shown above these values. Residues mutated in this and in our previous study are circled. The standard numbering for some of the GlyR M2 residues is shown in brackets. The sequences are taken from: (a) Grenningloh et al. (1987), (b) Schofield et al. (1987), (c) Keramidas et al. (2000), and (d) Couturier et al. (1990).

tamate (or arginine) residues are exposed to permeating ions at the intracellular mouth of the α, β, and δ subunits of nAChRs of *Torpedo* (Imoto et al., 1988), mouse muscle (Wilson and Karlin, 2000), and 5-HT$_3$Rs (Reeves et al., 2001). The charge at the extracellular channel mouth of LGICs is more variable. For instance, the α1 subunits of the GlyR and the α1, β1, and γ2 subunits of GABA$_A$Rs present positively charged residues to the extracellular mouth of the ion channel at position 19'. However, an uncharged alanine in the β subunit of the GlyR and glycine in the ρ1 subunit of the GABA$_C$R occupy this position. Similarly, the extracellular border of the cation-selective LGIC pores varies with the 5-HT$_{3A}$Rs and the α, β1, and β3 subunits of nAChRs having negatively charged glutamate or aspartate residues, whereas the vertebrate β2, β4, δ, γ, and ε subunits of nAChRs have either glutamine or lysine residues at position 20'. The β1, γ, δ, and ε subunits of nAChRs have either lysine or arginine residues at position 21' (Le Novère and Changeux, 1999, and their web database at http://www.pasteur.fr/recherche/banques/LGIC/LGIC.html). The role of these rings of charged amino acids flanking the transmembrane channel in LGICs has been well documented. Mutations reducing the positively charged extracellular ring in α1 homomeric GlyRs result in a decrease in single channel conductance and a partial disruption of the channel gating mechanism (Langosch et al., 1994; Rajendra et al., 1995). In *Torpedo californica* nAChRs, Imoto et al. (1988) showed that reducing the magnitude of the charge of these rings proportionally reduced the magnitude of the single channel conductance, the greatest change occurring for mutations in the intermediate ring. These results suggest that the intermedi-

ate ring corresponds to a region of the pore that is constricted enough to closely interact with permeating ions. Cysteine-scanning mutagenesis later supported this inference by providing evidence that both the rat nAChR (Wilson and Karlin, 1998) and the $GABA_AR$ (Xu and Akabas, 1996) channels taper to a constriction in the region of the intermediate ring.

Mutagenesis of the intermediate ring of charge has also implicated this region as being important as the ion-charge selectivity filter in LGICs. Galzi et al. (1992) converted the α7 homomeric nAChR from being cation- to anion-selective by mutating a minimum of three residues found in the wild-type (WT) α7 nAChR subunit to those found in the equivalent positions in the α1 GlyR subunit. These M2 mutations consisted of the insertion of a proline, −2'P, and the substitutions, E-1'A and V13'T. Two of these mutations, (−2'P and E-1'A), are in the region of the pore constriction. Subsequent studies on anion-selective α7 nAChR mutants (Corringer et al., 1999) have led to two deductions. First, that the critical mutation for conferring anion selectivity to the α7 nAChR was the proline insertion (−2'P), which, when combined with E-1'A and V13'T, could be inserted in positions −1', −2', or −4' to give anion-selective channels. And second, that the electrostatic environment at the pore constriction required for charge selectivity is contributed by the peptide backbone rather than the charged amino acid side chains. Recently, the three inverse mutations in the α1 homomeric GlyR have been shown to convert that channel from being anion- to cation-selective (Keramidas et al., 2000; selectivity triple mutant [STM] GlyR; Fig. 1). The murine $5\text{-}HT_{3A}R$ homomers have also been successfully converted to anion-selective using the same three mutations as those of the α7 nAChR (Gunthorpe and Lummis, 2001; see also Gunthorpe et al., 1996). The fact that the same residue positions and reciprocal mutations switch the ion-charge preference of these LGICs strongly suggests that the mechanism of ion-charge selectivity is conserved in the LGIC superfamily.

A notable difference, however, between the cation-selective STM GlyR mutant and the WT α7 nAChR is that the latter has a substantial calcium permeability, whereas in the STM GlyR mutant no calcium permeability was detected. Bertrand et al. (1993) identified discrete sites within the M2 domains of the α7 nAChR that profoundly affect calcium permeability. One of these sites is located at the intermediate ring, where the neutralization of the negative charge (E-1'A) abolished calcium permeability, suggesting that this region is also important for divalent ion permeation. The same study identified two other regions, located toward the extracellular end of the channel, (L16', L17', and V13'), that significantly altered Ca^{2+} permeability. Mutations to L16' or L17' abolished Ca^{2+} permeability, whereas V13'T greatly accentuated Ca^{2+} permeability. These results suggest that Ca^{2+} ion permeation requires interactions with pore residues besides those found at the pore constriction, but whether this feature is conserved in the LGIC family is unknown.

The use of permeant organic ions of different sizes as an investigative tool to determine minimum channel pore dimensions has been used extensively for a variety of ion channels, including the members of the nicotinic AChR family of LGICs. It has been reported previously that the cation-selective nAChRs have a minimum pore diameter ranging between 0.74 nm in *Rana pipiens* muscle (Dwyer et al., 1980) and *Torpedo californica* (Wang and Imoto, 1992) to 0.84 nm in mouse muscle (Cohen et al., 1992a). Studies of $5\text{-}HT_3Rs$ also report a pore diameter for this channel of 0.76 nm (Yang, 1990). In contrast, the anion-selective GlyRs and γ-aminobutyric acid receptor (GABARs) channels appear to have smaller minimum pore diameters. Native rat spinal cord GlyRs and GABARs have minimum pore diameters of 0.52 and 0.56 nm, respectively (Bormann et al., 1987), which is similar to values found later for native GlyRs and GABARs found in rat hippocampal neurons (Fatima-Shad and Barry, 1993). Human recombinant α1 homomeric and α1/β heteromeric GlyRs have comparable pore diameters of 0.53 and 0.52 nm, respectively (Rundstrom et al., 1994), whereas the homomeric ρ1 $GABA_CR$ is reported to have a pore diameter of 0.61 nm (Wotring et al., 1999). Hence it is conceivable that the diameter of the ion channel in LGICs may, in part, govern ion-charge selectivity.

The aim of the present investigation was to elucidate residues within the ion conduction pathway that comprises the selectivity filter of the α1 GlyR. In particular, we endeavored to determine whether two, or even one, M2-domain point mutations in the constricted region of the pore were sufficient to convert the GlyR channel from being anion- to cation-selective and to change the diameter of these ion pores. We also wished to investigate the role of the extracellular ring of charge at the channel entrance in divalent and monovalent ion permeability.

MATERIALS AND METHODS

Transient Expression of Recombinant α1 Subunit GlyRs in HEK293 Cells

Complementary DNA (cDNA) encoding the α1 subunit of the human GlyR was subcloned into the pCIS expression vector. Site-directed point mutations in the cDNA were constructed using the oligonucleotide-directed PCR mutagenesis method of Ho et al. (1989). The cDNA clones were subsequently confirmed by sequencing and transfected using the calcium phosphate precipitate method of Chen and Okayama (1987). The procedure resulted in transient expression of α1 homopentameric GlyRs. The HEK293 cells were cotransfected with the cDNA encoding the CD4 surface antigen, enabling them to be labeled with CD4-

coated polystyrene beads (Dynabeads M-450, CD-4; Dynal). The dynabead labeling acted as a transfection marker and aided in cell selection for the electrophysiological experiments. Five α1 GlyR mutant channels were investigated in this study, all of which had point mutations flanking the M2 transmembrane domain (Fig. 1). These were: (a) the SDM GlyR with P-2'Δ (P250Δ) and A-1'E (A251E); (b) the single A-1'E (A251E) mutant GlyR; (c) the single P-2'Δ (P250Δ) mutant GlyR; (d) the SDM+R19'A GlyR, with P-2'Δ (P250Δ), A-1'E (A251E), and R19'A (R271A); and (e) the SDM+R19'E GlyR, with P-2'Δ (P250Δ), A-1'E (A251E), and R19'E (R271E).

Solutions

The standard intracellular (pipette) solution consisted of (in mM): 145 NaCl, 10 HEPES, 2 $CaCl_2$, and 5 EGTA titrated to a pH of 7.35 with NaOH. Three extracellular (bath) solutions were used for the dilution potential experiments. The solution that was approximately symmetrical (1NaCl) with the intracellular solution consisted of (in mM): 145 NaCl, 10 HEPES, 10 glucose. The first dilution (0.5NaCl) consisted of (in mM) 75 NaCl, 10 HEPES, 10 glucose, and 136 sucrose, whereas the second dilution (0.25NaCl) consisted of (in mM) 37.5 NaCl, 10 HEPES, 10 glucose, and 189 sucrose. Sucrose was added to the NaCl diluted solutions in order to maintain equiosmolar conditions. Biionic potential experiments were used to determine the permeability of alkali cations in the SDM GlyRs and organic cations (for convenience we refer to NH_4^+ as an "organic" cation) in A-1'E, SDM, SDM+R19'A, and SDM+R19'E GlyRs. Here, the control solution used was the 1NaCl solution described above. The cation test solutions were similar to the 1NaCl solution except that the NaCl was replaced with a test cation salt. That is, 145 mM of CsCl, RbCl, KCl, LiCl, NH_4Cl, TriMAHCl (Trimethylammonium chloride), TMACl (Tetramethylammonium chloride), TrisHCl (Tris[Hydroxymethyl]aminomethane hydrochloride), TEACl (Tetraethylammonium chloride), or TPACl (Tetrapropylammonium chloride). Biionic potential experiments were also used to test the permeability of Ca^{2+} ions in SDM, SDM+R19'A, and SDM+R19'E GlyRs. The Ca^{2+} test solution consisted of (in mM): 50 $CaCl_2$, 53 NaCl, 10 HEPES, and 10 glucose with the control solution being the 1NaCl solution described above. All extracellular solutions were titrated to a pH of 7.40 with NaOH. Originally, the dilution potential experiments in addition to the alkali cation test experiments for SDM GlyRs were done in intra- and extracellular solutions containing 2 mM $CaCl_2$ and 2 mM $MgCl_2$. In a series of later experiments, these divalent cations were omitted and the divalent-free 0.5NaCl (standard) solution was tested and compared with the divalent-containing 0.5NaCl solution (see RESULTS). Supramaximal response glycine concentrations were used for all experiments and were achieved by dissolving the appropriate amount of glycine in the extracellular solutions. The glycine concentrations used were (in mM): 50 or 30 for SDM, 30 for SDM+R19'A, 50 or 30 for SDM+R19'E and 20 for the P-2'Δ and A-1'E GlyRs. WT single channel currents were elicited using a glycine concentration of 1 μM or less, depending on the level of single channel activity. The solutions were delivered to the recorded cell via a parallel array of gravity-fed plastic microperfusion tubes, which were mounted on a 3-axis electromechanical manipulator (Marzhauser Wetzlar, DC-3K; SDR Clinical Technology).

Electrophysiology

Whole-cell recordings. All experiments were performed in voltage-clamp mode and at laboratory temperature (21 ± 1°C). Patch pipettes were made using borosilicate haematocrit tubes (Vitrex-1601; Herlev), pulled on a two-stage electrode puller (Sutter Instruments Co.), and fire-polished. When filled with pipette solution, their resistances ranged between 1.5–2.8 MΩ. Whole-cell currents were recorded using an Axopatch-1D amplifier, digitized by a Digidata 1200 A/D board, and recorded using *pClamp 8.0.3* software (all from Axon Instruments, Inc.) on a 166 MHz Pentium computer. Current recordings were filtered with a 4-pole Bessel filter that was built into the amplifier at a −3 dB value of 200 Hz and acquired at a sampling frequency of 1 or 2 kHz. Prior to establishing the whole-cell configuration, seal resistances ranged between 1.2–6.0 GΩ. Series resistances ranged between 2–10 MΩ and were compensated for by 50–65% with the amplifier. Experiments with a series resistance greater than 10 MΩ were aborted. Patch electrodes were tested after each experiment for drift in the electrode tip potential, which was corrected if it exceeded ±1 mV (<5% of all experiments and never exceeding ±1.8 mV). Two equivalent recording voltage protocols were used (e.g., Fig. 4). The first involved setting the membrane voltage, using the amplifier, to values of (in mV): −60, −40, −20, 0, 20, 40, and 60 and eliciting glycine-activated currents at each voltage (see Fig. 4, right). Here, peak current amplitude was measured at each membrane voltage to generate the I-Vs. Alternatively, a *pClamp*-generated voltage-step protocol was used. This involved first testing for glycine-activated current expression in the recorded cell at a holding potential of −40 mV before switching the amplifier voltage setting to zero and initiating the step protocol, which stepped the membrane voltage between −60 mV to 60 mV at 20 mV intervals (see Fig. 4, left). Each voltage step lasted for 160 ms. The voltage steps were initiated during the steady-state macroscopic current, which corresponded to ~2 s after the onset of glycine. Since the current during the voltage steps showed no obvious decay, the amplitude was averaged over the duration of each step. These voltage steps were first applied to the baseline current (absence of agonist) and then to the glycine-activated current. For both recording protocols glycine was washed on the cell for a period of 4–5 s using the relatively fast perfusion system described above, which has an estimated solution exchange time of 15–20 ms. For the dilution potential experiments, all three extracellular NaCl concentrations were tested on the same cell. Each biionic experiment, which consisted of a measurement in control (1NaCl) and a test cation solution, was also done on the same cell. In nearly all cases, repeat experimental runs were performed on each cell to check for consistency in the reversal potential for each extracellular solution.

Single channel recordings. Outside-out membrane patches were excised from cells expressing WT α1 GlyRs using electrodes pulled from thick-walled glass capillaries (Clark Electrical Instruments). The electrodes' tips were also coated with Sylgard (Dow Corning) and fire-polished. The resistance of the patch electrodes ranged between 9–12 MΩ when filled with pipette solution. Patch seal resistances ranged between 6–40 GΩ. The recording equipment and experimental conditions were identical to those described for the whole-cell recordings, with the exception being that the recordings were filtered at 2 kHz and acquired at a sampling frequency of 10 kHz. The experimental protocol involved holding the membrane patch at voltages between −60 to 60 mV at 20-mV intervals and recording glycine-activated single channel currents at each voltage. All three extracellular NaCl solutions were tested on the same patch with the exception of one set of data, which combined two experiments.

Analysis

Offline analysis and graphing was done using *pClamp 8* or *SigmaPlot 5.0* (Jandell Scientific). Liquid junction potentials were corrected by using the Windows version of the *JPCalc* software (Barry, 1994). I-V plots were generated for each experimental run. Single

channel currents were measured directly using *pClamp*. The most frequently occurring conductance state, which was usually the largest, was chosen for constructing the I-V plot. For the whole-cell recordings, which used *pClamp*-generated voltage steps, the baseline currents were subtracted from those in the presence of glycine before plotting the net glycine-activated currents. For all I-Vs, the data points were then fitted to quadratic polynomials (occasionally to third order polynomials) and the reversal potential read directly from the I-V plots. For the dilution potential experiments, the permeability ratio (P_{Cl}/P_{Na}) was calculated for each experiment and then averaged for each mutant. For the alkali cation (P_X/P_{Na}), calcium (P_{Ca}/P_{Na}), and organic cation (P_X/P_{Na}) permeability ratios, the reversal potentials were pooled for each experiment type and averaged. The averaged values ($\bar{v}_{rev}$) were then used to calculate the permeability ratios. Ion activities, rather than concentrations, were used for all P_{Cl}/P_{Na} and P_{Ca}/P_{Na} calculations and for P_X/P_{Na} for the alkali cation calculations. Activities were determined by graphing and interpolating published values (Robinson and Stokes, 1965). All data is expressed as mean ± SEM. For the dilution potential experiments the Goldmann-Hodgkin-Katz (GHK) equation was used to calculate the values of P_{Cl}/P_{Na}:

$$V_{rev} = (RT/F)\mathrm{In}([a_{Na}^{\circ} + \{P_{Cl}/P_{Na}\}a_{Cl}^{i}]/[a_{Na}^{i} + \{P_{Cl}/P_{Na}\}a_{Cl}^{\circ}]) \quad (1)$$

where V_{rev} is the potential at which the current is zero, R is the Gas constant, T is temperature in Kelvin, F is Faraday's constant, P_{ion} is the permeability of the ion, and a_{ion} is the activity of the ion in the extracellular (°) or intracellular (i) solution. The P_X/P_{Na} ratios for alkali cations and organic cations were calculated using a modified form of the GHK equation:

$$\begin{aligned}\Delta V_{rev} &= V_{rev}^{T} - V_{rev}^{C} \\ &= (RT/F)\mathrm{In}([a_{Na}^{\circ T} + \{P_X/P_{Na}\}a_X^{\circ} + \\ &\quad \{P_{Cl}/P_{Na}\}a_{Cl}^{i}]/[a_{Na}^{\circ C} + \{P_{Cl}/P_{Na}\}a_{Cl}^{i}])\end{aligned} \quad (2)$$

where the superscripts T and C denote test cation solution and control (symmetrical) solutions, respectively, and the $[a_{Na}^{i} + (P_{Cl}/P_{Na})a_{Cl}^{o}]$ term for both solutions will essentially cancel out since $a_{Cl}^{o} \sim a_{Cl}^{i}$. X represents the test monovalent cation.

The P_{Ca}/P_{Na} values were calculated using the generalized Goldman current equation for permeant ions at zero current (e.g., Barry and Gage, 1984):

$$I = \Sigma_j P_j z_j^2 (V_{rev}F^2/RT)([a_j^{\circ} - a_j^{i}\exp\{z_j V_{rev}F/RT\}]/[1 - \exp\{z_j V_{rev}F/RT\}]) = 0 \quad (3)$$

where P_j and z_j are the permeability and valency of ion j, respectively, I is the current, and (°) and (i) again denote extracellular and intracellular solutions, respectively.

Minimum pore diameter estimates were obtained from organic cation permeability calculations using Eq. 2 above, where the concentrations of the permeant ions were used instead of their activities. The activities of the organic cations did not need to be used because the ionic strength was constant and there was not expected to be a significant difference in activity coefficients between the cations. The minimum pore diameter estimates were based on the principle that the permeability of an ion is proportional to the cross-sectional area of the most constricted part of the pore left unoccupied as an ion traverses through it (excluded area theory; Dwyer et al., 1980). Therefore, P_X/P_{Na} can be expressed as:

$$P_X/P_{Na} = ([d_P - d_X]/[d_P - d_{Na}])^2 \quad (4)$$

where P_X/P_{Na} is the permeability ratio of the organic cation relative to Na^+, d_P, d_X, and d_{Na} are the diameters of the pore, organic cation, and Na^+, respectively (Cohen et al., 1992a; where we are using diameters rather than radii).

Eq. 4 can be manipulated so that:

$$\sqrt{P_X/P_{Na}} = y_o - m d_X \quad (5)$$

where $y_0 = d_P/(d_P - d_{Na})$ and $m = 1/(d_P - d_{Na})$.

The relationship between P_X/P_{Na} and d_P according to Eq. 5 is illustrated in Fig. 8. The pore diameter can be obtained using the slope (m) and y-intercept (y_0), since $d_P = y_0/m$.

RESULTS

General Current Properties of Cation-selective Mutant α1 GlyRs

HEK293 cells transiently transfected with the α1 GlyRs; SDM (P-2'Δ, A-1'E), A-1'E, P-2'Δ, SDM+R19'A (P-2'Δ, A-1'E, R19'A), and SDM+R19'E (P-2'Δ, A-1'E, R19'E) typically exhibited current amplitudes between 300 pA to 15 nA. The amplitude of glycine-elicited currents showed a positive correlation with the level of CD4 antibody labeling. These current amplitudes were comparable with those observed previously in HEK293 cells expressing WT α1 GlyRs under the same conditions (Keramidas et al., 2000). A saturating concentration of glycine was used for all experiments (20–50 mM; see MATERIALS AND METHODS), which was chosen on the basis of concentration-response experiments performed on the mutant GlyRs (Moorhouse et al., 2002, this issue) and suggested that the EC_{50} for all mutant GlyRs was increased compared with WT α1 GlyRs (EC_{50} ~30 μM; Rajendra et al., 1994). However, the restoration of the T13' in the mutant receptors enhanced channel activation (or agonist binding) compared with the STM GlyR (Keramidas et al., 2000), as suggested by the two- to fivefold lower agonist concentrations used for the present GlyR mutant channels. Whole-cell I-V experiments also revealed that macroscopic current rectification varied amongst the cation-selective mutant GlyRs. The observed macroscopic current rectification could arise from voltage-dependent changes in open probability and/or single channel conductance. However, the macroscopic rectification observed for the mutant GlyRs is consistent with, and primarily attributed to, the single channel current rectification (Moorhouse et al., 2002, this issue).

As relatively high glycine concentrations were used on the GlyR mutants, a test was undertaken to determine whether the reversal potentials would be affected by the osmotic change in the glycine-containing solutions. Two supramaximal agonist, "0.5NaCl" solutions were tested on the same cells expressing the SDM GlyR. One solution contained 10 mM glycine, whereas the other contained 50 mM glycine, the osmotic difference being 40 mosm. There was no

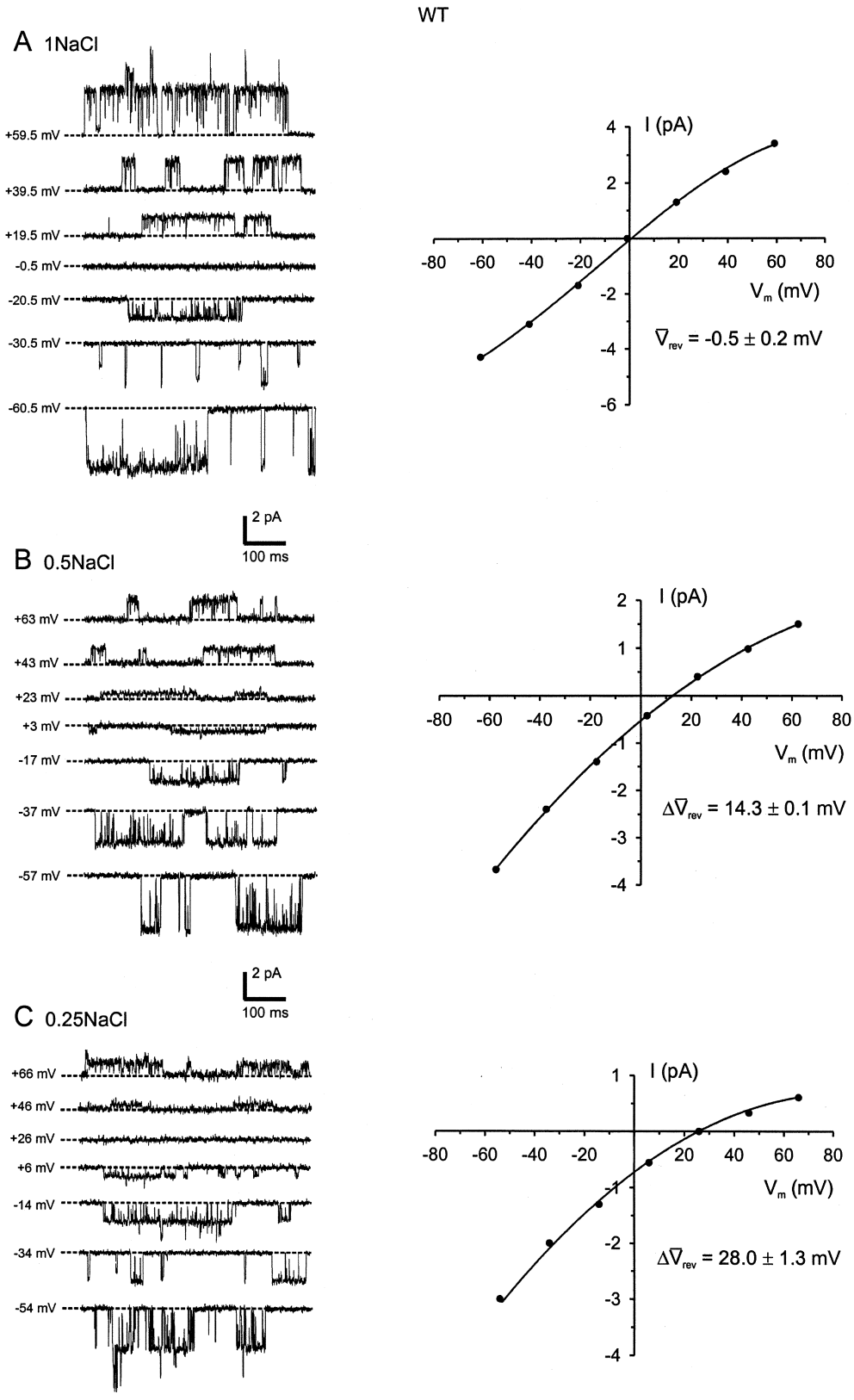

FIGURE 2. WT single channel dilution I-Vs. An example of a dilution potential experiment for WT α1 GlyRs. All single channel traces were recorded from the same patch at the membrane potentials indicated (corrected for liquid junction potentials). The dashed lines represent the closed state of the channels. I-Vs were plotted for each extracellular NaCl solution described in the legend to Fig. 4, using the amplitude of the main state conductance level for each recording. The data points were fitted to quadratic polynomials. Also quoted are the average reversal potential measurements ($\Delta\bar{V}_{rev}$, $n = 3$) for each extracellular NaCl concentration used. Currents were further low-pass filtered offline at 1 kHz.

significant difference in the reversal potentials between the two glycine-containing solutions ($\Delta V_{rev} = -1.0 \pm 0.6$ mV, $n = 4$, paired t test, $P = 0.17$).

Dilution Potentials for α1 GlyR Mutants

To determine the relative anion-cation permeability ratio, the extracellular NaCl concentration was initially di-

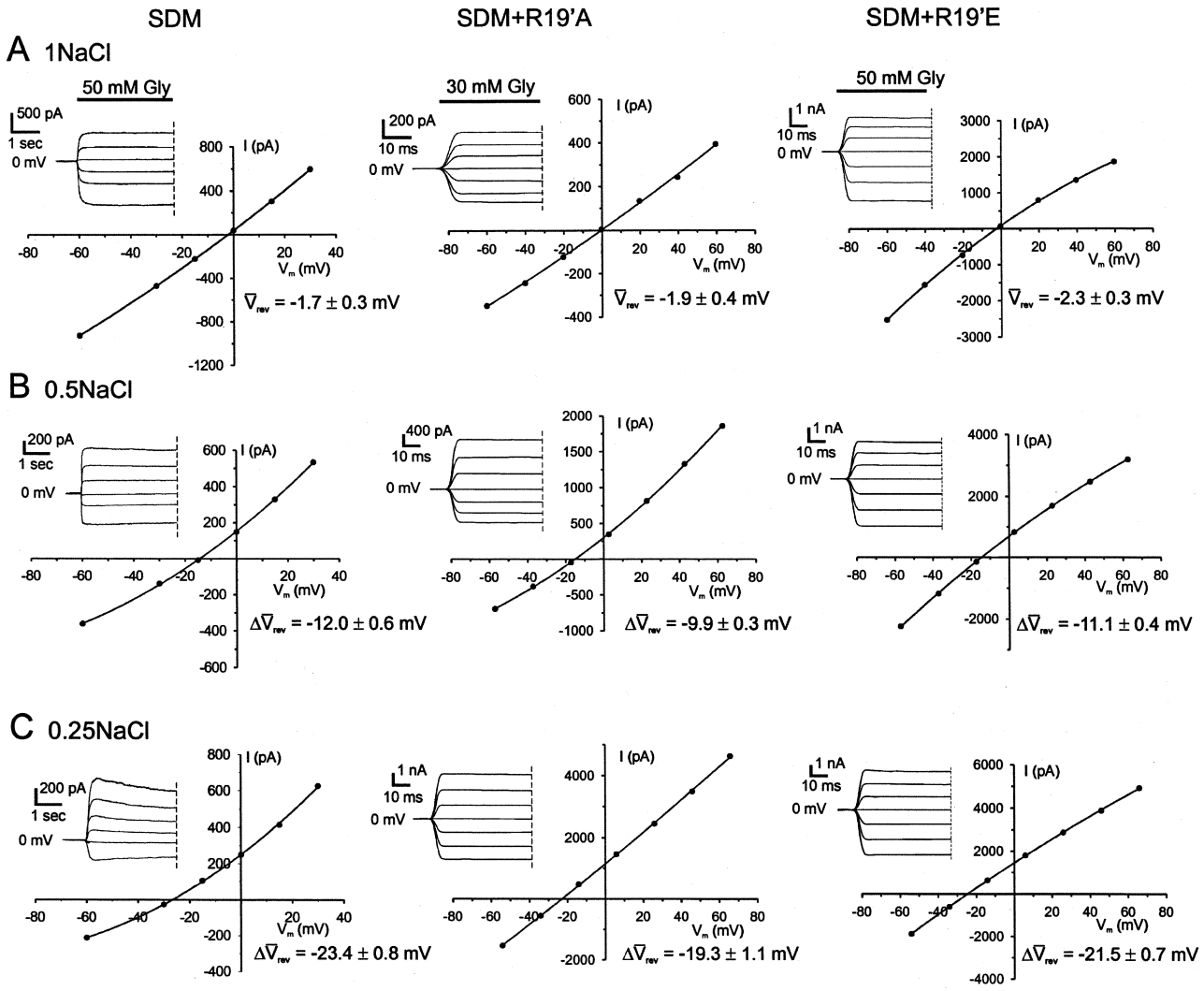

FIGURE 3. Sample dilution I-Vs for the cation-selective SDM, SDM+R19'A, and SDM+R19'E α1 GlyRs. Examples of dilution potential experiments for the SDM-based cation-selective GlyRs with their accompanying glycine-activated current responses. Each column of I-Vs was recorded from the same cell, as the extracellular NaCl was diluted from ~150 mM (A, 1NaCl) to ~80 mM (B, 0.5NaCl) and finally to ~40 mM (C, 0.25NaCl). For the SDM, GlyR experiments the concentrations of ions present in the intracellular (pipette) solutions were (in mM): 163 Na^+, 153 Cl^-, 2 Mg^{2+}, 2 Ca^{2+}, and 5 EGTA. All three extracellular solutions contained 10 mM HEPES, 2 mM Ca^{2+}, and 2 mM Mg^{2+}, with the 1NaCl solution also containing 149.5 mM Na^+ and 153 mM Cl^-. The 0.5NaCl solution also contained 75.9 mM Na^+ and 83 mM Cl^-, whereas the 0.25NaCl solution also contained 42.1 mM Na^+ and 45.5 mM Cl^-. The solutions used for SDM+R19'A and SDM+R19'E GlyRs were simplified by omitting $CaCl_2$ and $MgCl_2$ from the extracellular solution and $MgCl_2$ from the intracellular solution (see legend to Fig. 4). The data points were fitted to quadratic polynomials. Also quoted are the average shifts in reversal potential measurements ($\Delta\bar{v}_{rev}$) for the SDM ($n = 8$), the SDM+R19'A ($n = 12$), and SDM+R19'E ($n = 7$) for each extracellular NaCl concentration used. Currents were further low-pass filtered offline at 100 Hz.

luted from ~145 mM to 75 mM and then to 37.5 mM, and the relative displacement of the zero current potential (reversal potential, V_{rev}) was measured. Fig. 2 shows an example of an I-V experiment performed on WT GlyRs using single channel currents from the same outside-out membrane patch. The I-V plots show a prominent rightward displacement in V_{rev} with decreasing extracellular NaCl, confirming that WT currents are carried mainly by Cl^- ions. Similarly, dilution potential experiments on the P-2'Δ GlyR produced a shift in the positive direction, although the degree of the shift was smaller than for the WT GlyRs, indicating that the P-2'Δ GlyR remained marginally anion-selective (Fig. 4, left).

In contrast, Figs. 3 and 4 (right) show examples of I-V plots with accompanying glycine-activated currents recorded for five GlyR mutants. As can be seen, as the concentration of extracellular NaCl progressively falls, there is a concomitant leftward shift in the reversal potential for SDM, SDM+R19'A, SDM+R19'E, and A-1'E GlyRs. The V_{rev} shifts are now in the direction of the

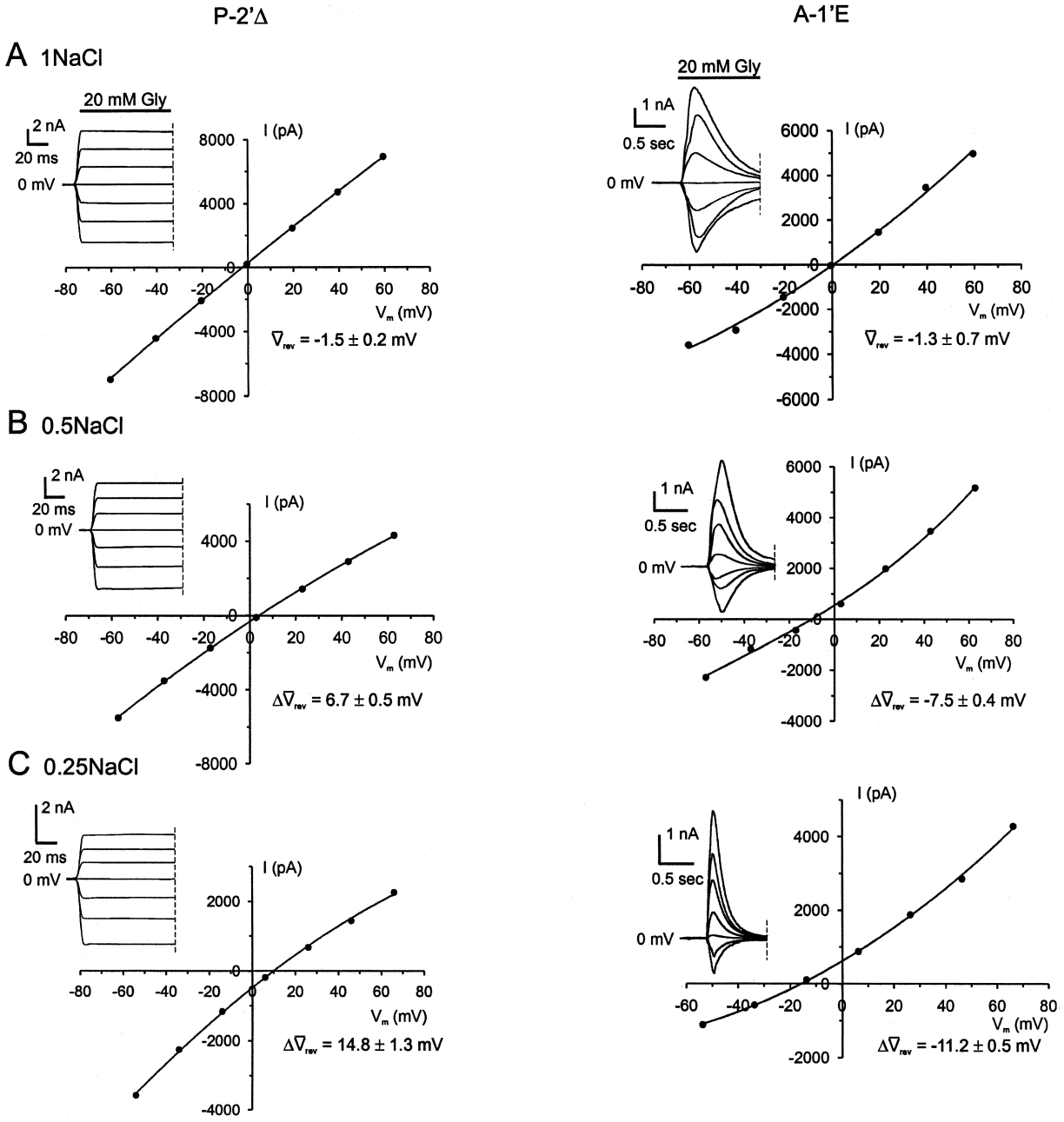

FIGURE 4. Sample dilution I-Vs for P-2'Δ and A-1'E α1 GlyRs. Examples of dilution potential experiments for the anion-selective P-2'Δ GlyR and the cation-selective A-1'E GlyR mutants with their accompanying glycine-activated current responses. Each column of I-Vs was recorded from the same cell. The concentrations of ions present in the intracellular (pipette) solutions were (in mM) 163 Na^+, 149 Cl^-, 2 mM Ca^{2+}, and 5 EGTA. All three extracellular solutions contained 10 mM HEPES with the 1NaCl (A) solution also containing 149.5 mM Na^+ and 145 mM Cl^-. (B) The 0.5NaCl solution contained 75.9 mM Na^+ and 75 mM Cl^-. (C) The 0.25NaCl solution contained 41.9 mM Na^+ and 37.5 mM Cl^-. The data points were fitted to quadratic polynomials. Also quoted are the average shifts in reversal potential measurements ($\Delta\bar{v}_{rev}$) for the P-2'Δ ($n = 8$), and A-1'E ($n = 6$) for each extracellular NaCl concentration used. Currents were further low-pass filtered offline at 100 Hz.

equilibrium potentials for Na^+, as predicted by the Nernst equation, indicating that these mutant channels are all predominantly Na^+ selective.

Due to the Ca^{2+} permeability through SDM GlyRs (see below), two "0.5NaCl" extracellular NaCl solutions were tested on the SDM GlyR channels. These solutions differed in that one contained 2 mM Ca^{2+} and 2 mM Mg^{2+} ions, whereas the other did not. The test was undertaken to determine the accuracy of dilution potential experiments for the SDM GlyR, which were originally done using solutions containing divalent cations. The averaged reversal potential shifts between the diva-

lent cation containing and divalent cation–free extracellular solutions were not significantly different ($\Delta V_{rev} = -12.0 \pm 0.6$ mV, $n = 8$ and $\Delta V_{rev} = -11.1 \pm 1.2$ mV, $n = 4$, respectively, unpaired t test, $P = 0.51$). Therefore, we concluded that the low Ca^{2+} permeability of the SDM GlyRs and the presence of relatively low concentrations of divalent cations in our original dilution potential experiments would result in the 2 mM Ca^{2+} not making a detectable impact on the reversal potential values we obtained.

Determination of Anion-Cation Permeability Ratios, (P_{Cl} /P_{Na}), for Cation-selective α1 GlyR Mutants

To calculate the values of P_{Cl}/P_{Na} for each GlyR, the GHK equation (Eq. 1) was fitted to the shift in V_{rev} (ΔV_{rev}) for each experiment. The individually calculated P_{Cl}/P_{Na} values were then averaged for each of the mutant GlyRs. The P_{Cl}/P_{Na} value obtained for the P-2'Δ GlyR was 3.8 ± 0.4 ($n = 8$), and that for the SDM GlyR was 0.13 ± 0.02 ($n = 8$), which is close to the P_{Cl}/P_{Na} value for the WT α7 nAChR ($P_{Cl}/P_{Na} = 0.1$; Bertrand et al., 1993). The value for the A-1'E GlyR was 0.34 ± 0.04 ($n = 6$), that for the SDM+R19'A GlyR was 0.23 ± 0.02 ($n = 12$), and that for the SDM+R19'E GlyR was 0.19 ± 0.02 ($n = 7$, Table I). Fig. 5 illustrates the averaged $\Delta\bar{V}_{rev}$ values for each GlyR against the logarithm of the permeant ion activity and shows a nearly linear relationship, suggesting little dependence of P_{Cl}/P_{Na} ratios on ion concentration. Fig. 5 B also shows the fit for WT GlyRs, the experiments for which were performed on excised membrane patches. The P_{Cl}/P_{Na} ratio for these experiments was 27.9 ± 1.3 ($n = 3$), which is comparable to the value of 24.6 obtained under similar conditions for WT GlyRs using whole-cell recordings (Keramidas et al., 2000).

Permeability of Alkali Cations in the SDM GlyR

Biionic potential experiments were performed on the SDM GlyR channels to determine relative alkali cation permeabilities. For each recorded cell, glycine-activated currents were recorded for a range of membrane voltages, in a control (symmetrical) NaCl solution, before the extracellular solution was replaced with one containing approximately the same concentration of test cation. The test cations examined were Cs^+, Rb^+, K^+, and Li^+. The averaged set (control, test cation, and relative shift) of reversal potentials for the alkali cations were (in mV): −1.5 ± 0.6, 9.3 ± 0.9, 10.8 ± 0.5 for Cs^+ ($n = 7$); −1.1 ± 0.4, 8.8 ± 0.6, 9.9 ± 0.4 for Rb^+ ($n = 9$); −0.4 ± 0.5, 8.1 ± 0.3, 8.5 ± 0.3 for K^+ ($n = 7$); and −0.1 ± 0.5, −5.4 ± 0.6, −5.3 ± 0.3 for Li^+ ($n = 9$). Using the shifts in reversal potential, the permeability of test cation relative to Na^+ was calculated using Eq. 2. These calculations yielded permeability ratios (P_X/P_{Na}), where X is the test cation, of: 1.70 ± 0.04, 1.61 ± 0.03, 1.49 ± 0.02, 1.00, and 0.76 ± 0.01 for Cs^+, Rb^+, K^+, Na^+, and Li^+, which corresponds to an alkali cation permeability sequence of: $Cs^+ > Rb^+ > K^+ > Na^+ > Li^+$.

Hence, the cation-selective SDM GlyR discriminates relatively poorly between alkali cations, with low field

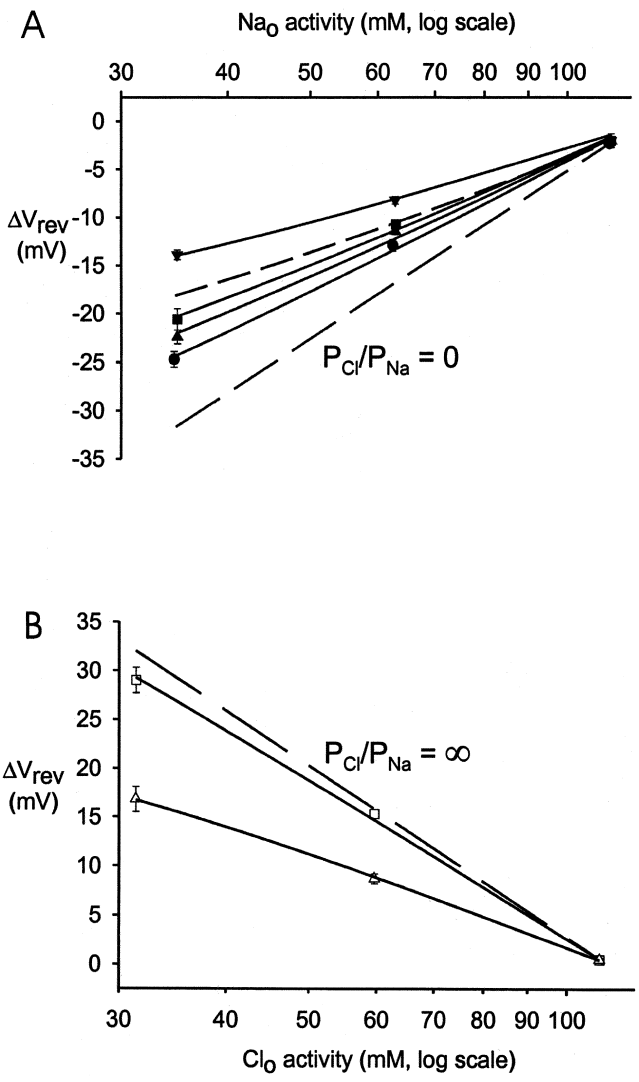

FIGURE 5. Permeability plots for the cation- and anion-selective α1 GlyRs. (A) Plots of the change in the averaged V_{rev} ($\Delta\bar{v}_{rev}$) as the extracellular NaCl solution was diluted against extracellular Na^+ activity ($a_{Na}{}^o$) for the cation-selective GlyR mutants. The data points were fitted to the GHK equation (Eq. 1). The long dashed line represents the GHK fit to E_{Na} for a hypothetical channel, which is exclusively permeable to Na^+ ions ($P_{Cl}/P_{Na} = 0$). The short dashed line is for comparison and represents the GHK fit for the STM GlyRs ($P_{Cl}/P_{Na} = 0.27$; Keramidas et al., 2000). For the SDM (●), $P_{Cl}/P_{Na} = 0.13$; for the SDM+R19'E (▲), $P_{Cl}/P_{Na} = 0.19$; for the SDM+R19'A (■), $P_{Cl}/P_{Na} = 0.23$; and for the A-1'E (▼), $P_{Cl}/P_{Na} = 0.34$. (B) Plots of the averaged ∇_{rev} ($\Delta\bar{v}_{rev}$) as the extracellular NaCl was diluted against extracellular Cl^- activity ($a_{Cl}{}^o$) for the anion-selective GlyRs. For P-2'Δ (Δ), $P_{Cl}/P_{Na} = 3.81$ and for WT (□), $P_{Cl}/P_{Na} = 27.9$. The long dashed line represents the GHK fit to E_{Cl} for a hypothetical channel that is exclusively permeable to Cl^- ions ($P_{Cl}/P_{Na} = \infty$).

strength interactions between permeating ion and pore residues. These results imply that low field strength interactions between permeating ion and pore residues are a common permeation property in both WT and cation-selective mutated GlyRs independent of the sign of the permeating ion. This permeation behavior is similar to that seen in native muscle nAChR channels with the same alkali-cation permeability sequence (Adams et al., 1980) and in the cation-selective STM GlyR mutant channel (Keramidas et al., 2000). In addition, native GlyRs and GABARs have been shown to have a low field strength sequence for halide ions (Bormann et al., 1987; Fatima-Shad and Barry, 1993; Wotring et al., 1999).

Permeability of Calcium in the SDM-based GlyRs

Biionic experiments were conducted to test the permeability of Ca^{2+} ions through the three SDM-based cation-selective GlyR channels. As shown in Table I and Fig. 6, all three cation-selective GlyR mutants tested showed some Ca^{2+} permeability, with the value for the SDM GlyR ($P_{Ca}/P_{Na} = 0.29 \pm 0.11$) being significantly lower than values for the SDM+R19'A ($P_{Ca}/P_{Na} = 0.73 \pm 0.20$) and the SDM+R19'E ($P_{Ca}/P_{Na} = 0.92 \pm 0.04$). The P_{Ca}/P_{Na} values for SDM+R19'A and SDM+R19'E GlyRs were not significantly different, although the P_{Ca}/P_{Na} value for SDM+R19'E did tend toward a higher Ca^{2+} permeability value. Furthermore, a notable and consistent observation during the experiments was that the inward current in high calcium solutions (carried mainly by Ca^{2+}) increased relative to inward Na^+ current from SDM to SDM+R19'A and then to SDM+R19'E (for the same driving force), implying that the charge of the extracellular ring affects Ca^{2+} conductance. In our previous study, the cation-selective STM GlyR mutant, which included the T13'V mutation, showed no detectable Ca^{2+} ion permeability (Keramidas et al., 2000).

Permeability of Organic Cations in Four Cation-Selective GlyRs

The permeabilities of organic cations were tested on four of the cation-selective GlyRs for the purpose of obtaining estimates of the minimum open pore diameters of these GlyRs. Fig. 7 shows an example of a test cation that is more permeant than Na^+ (NH_4^+, rightward shift in V_{rev}) and one that is less permeant than Na^+ (TEA^+, leftward shift in V_{rev}) for the three SDM-based GlyRs. In general, cation permeability decreased with increasing cation mean diameter with the exception of $Tris^+$, which was just as, or more, permeant than TMA^+ for all SDM-based GlyRs tested even though it has a larger mean diameter than TMA^+ (Table II). For SDM+R19'A and SDM+R19'E GlyRs, TPA^+ completely blocked glycine-activated inward currents, which precluded obtaining accurate I-V experiments for this cation. It was therefore concluded that TPA^+ was impermeant through these channels based on its glycine-activated current block. As shown in Fig. 8, Eq. 4 describes the data accurately, with the r^2 values for the fits of the complete set of data being 0.83 for A-1'E, 0.95 for SDM+R19'A, and SDM+R19'E and 0.92 for SDM GlyRs. The values for minimum pore diameters obtained from these fits for A-1'E, SDM, SDM+R19'A, and SDM+R19'E are (in nm): 0.65, 0.97, 0.82, and 0.83, respectively (Fig. 8, solid lines). All four values are larger than the diameter of the α1 WT GlyR, which is 0.53 nm (Rundstrom et al., 1994), with the SDM-based GlyRs being considerably larger and in close agreement with the value obtained for the mouse nAChRs 0.84 nm (Cohen et al., 1992a). In addition, the test cations that are capable of hydrogen bonding, NH_4^+, $TriMA^+$, and $Tris^+$ were plotted separately and gave minimum pore diameters for SDM, SDM+R19'A, and SDM+R19'E of (in nm): 0.93, 0.78, and 0.84, respectively (Fig. 8, long dashed lines). Organic cations that are incapable of hydrogen bonding, TMA^+, TEA^+, and TPA^+ yielded minimum pore diameters of (in nm): 1.1, 0.86, and 0.85 for SDM, SDM+R19'A, and SDM+R19'E, respectively (Fig. 8, short dashed lines).

TABLE I

Permeability Ratios for Cl^- and Ca^{2+} Relative to Na^+

α1 GlyR	P_{Cl}/P_{Na} (*n*)	P_{Ca}/P_{Na} (*n*)	Ion selectivity
WT	24.6 ± 0.7 (8)[a]		Anion
	27.9 ± 1.3 (3)[b]		
P-2'Δ	3.81 ± 0.4 (8)		Anion
A-1'E	0.34 ± 0.04 (6)		Cation
SDM	0.13 ± 0.02 (8)	0.29 ± 0.11 (6)	Cation
SDM+R19'A	0.23 ± 0.02 (12)	0.73 ± 0.20 (9)	Cation
SDM+R19'E	0.19 ± 0.02 (7)	0.92 ± 0.04 (8)	Cation

A summary of the anion-cation permeability ratios (P_{Cl}/P_{Na}), measured with dilution potentials, and the relative calcium to sodium permeability ratio, measured with biionic potentials (P_{Ca}/P_{Na}), for the WT and the five GlyR mutant channels.

[a]Value taken from Keramidas et al. (2000).

[b]Obtained from single channel recordings (see Fig. 4). Permeability ratios are stated as mean ± SEM.

DISCUSSION

Delineation of the Principal Charge Selectivity Filter in the α1 GlyR

Previous mutagenesis studies on the conversion of charge selectivity in α7 nAChRs required additional M2 mutations to those in the constricted region. The α7 nAChR mutant P-2' and E-1'A apparently failed to form functional channels and required the inclusion of V13'T or other hydrophilic residues at 13' or L9'T (Galzi et al., 1992; Corringer et al., 1999). Similarly, both the cation-selective α1 GlyR STM mutant (Keramidas et al., 2000) and the anion-selective 5-HT_{3A}R STM

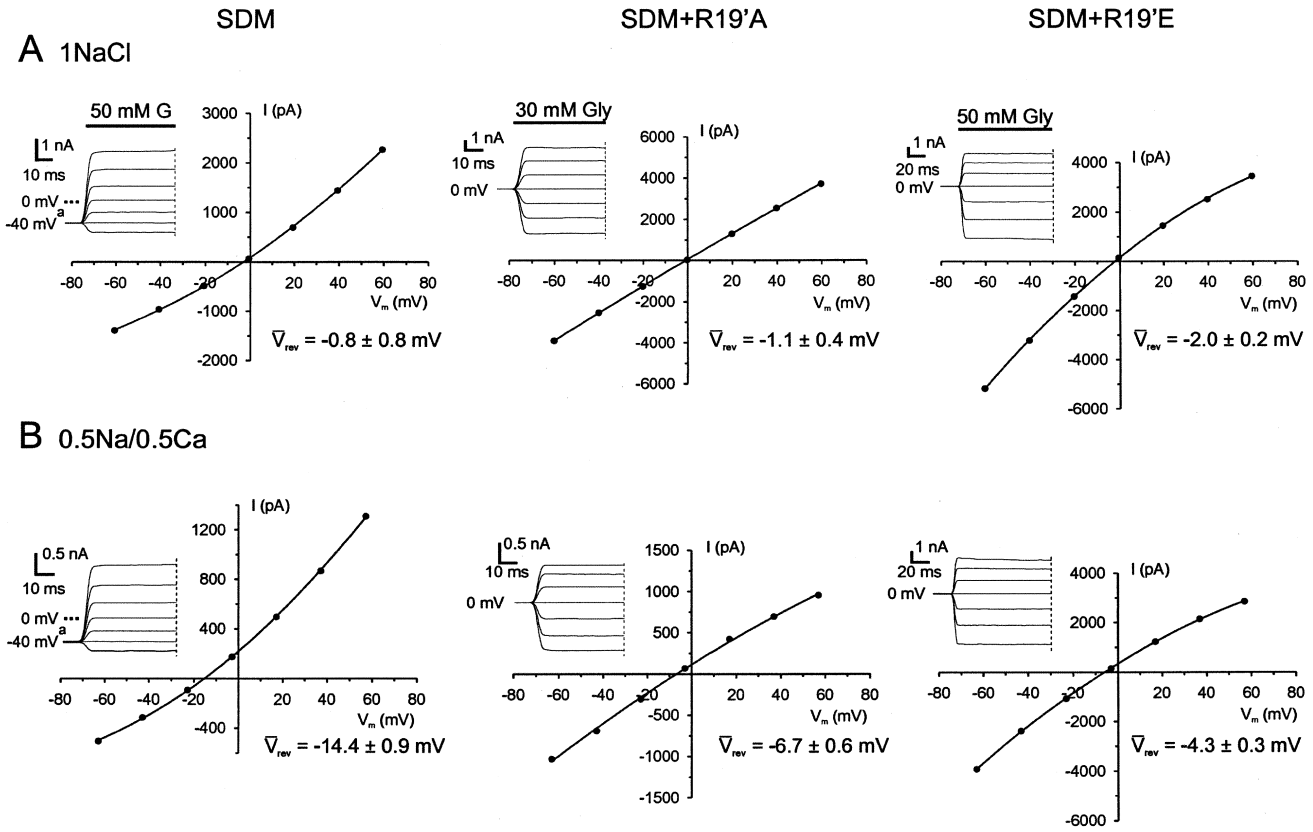

FIGURE 6. Sample biionic I-Vs for Ca^{2+} permeability. I-V plots and accompanying glycine-activated current responses for experiments testing the relative permeability of Ca^{2+} ions through the SDM-based cation-selective GlyR channels. Each column of the I-V pair was recorded from the same cell in ~150 mM NaCl (A, 1NaCl) and then a mixture of NaCl and $CaCl_2$ (B, 0.5Na/0.5Ca). The intracellular (pipette) and extracellular (control) solutions used for these experiments were the same as those described in the legend to Fig. 4 for each mutant. The Ca^{2+} test solution contained (in mM) 50 Ca^{2+}, 57.5 Na^+, and 153 Cl^-. The average reversal potentials ($\bar{v}_{rev}$) are also shown for the SDM ($n = 6$), SDM+R19'A ($n = 9$), and for SDM+R19'E ($n = 8$). The data points were fitted to quadratic polynomials. Relative permeability ratios (P_{Ca}/P_{Na}) were calculated using the generalized current–voltage equation for permeant ions at zero current (Eq. 3). Superscript a, voltage steps were applied from a holding potential of −40 mV. Currents were further low-pass filtered offline at 100 Hz.

mutant (Gunthorpe and Lummis, 2001) also included mutations at the 13' position in addition to the pore constriction region mutations, although other anion-selective mutations in the 5-HT_{3A}R channel have not been reported. The cation-selective GlyR mutants in this study (all of which retain T13') produced current amplitudes similar to those of WT α1 GlyRs and required agonist concentrations which were two- to fivefold lower than the glycine doses needed for the STM GlyR, which also had significantly smaller whole-cell currents. Moreover, not mutating the threonine residue in the SDM GlyR imparted a greater monovalent cation selectivity and a substantial Ca^{2+} selectivity (Table I), as the V13'T substitution did for the α7 nAChR (Bertrand et al., 1993). Hence, we postulate that the 13'V mutation is counterproductive for receptor activation and current amplitude in α1 GlyRs.

We now show unequivocally that charge selectivity conversion can be achieved solely with mutations in the constricted region of the α1 homomeric GlyR. Our results show that two adjacent point mutations (SDM; P-2'Δ, A-1'E) produce a GlyR channel with a significant preference for cations in contrast to the anion-selective WT. Hence, our results allow us to infer that the charge selectivity filter of the α1 GlyR is located in the region of the −1' and −2' positions, a result which agrees reasonably well with data from the nAChR (Cohen et al., 1992b). Galzi et al. (1992) and Corringer et al. (1999) proposed that the −2'P insertion in the anion-selective α7 nAChR triple mutant provided the local geometrical change to the pore constriction of that channel to allow anion-charge selectivity to take place. This is consistent with previous studies postulating that the proline at position −2' places geometrical constraints on the WT GlyR, which when mutated as the missense mutation P-2'T causes an alteration in peptide angle in that region (Saul et al., 1999). We concur with these hypotheses and suggest that the deletion of proline in our

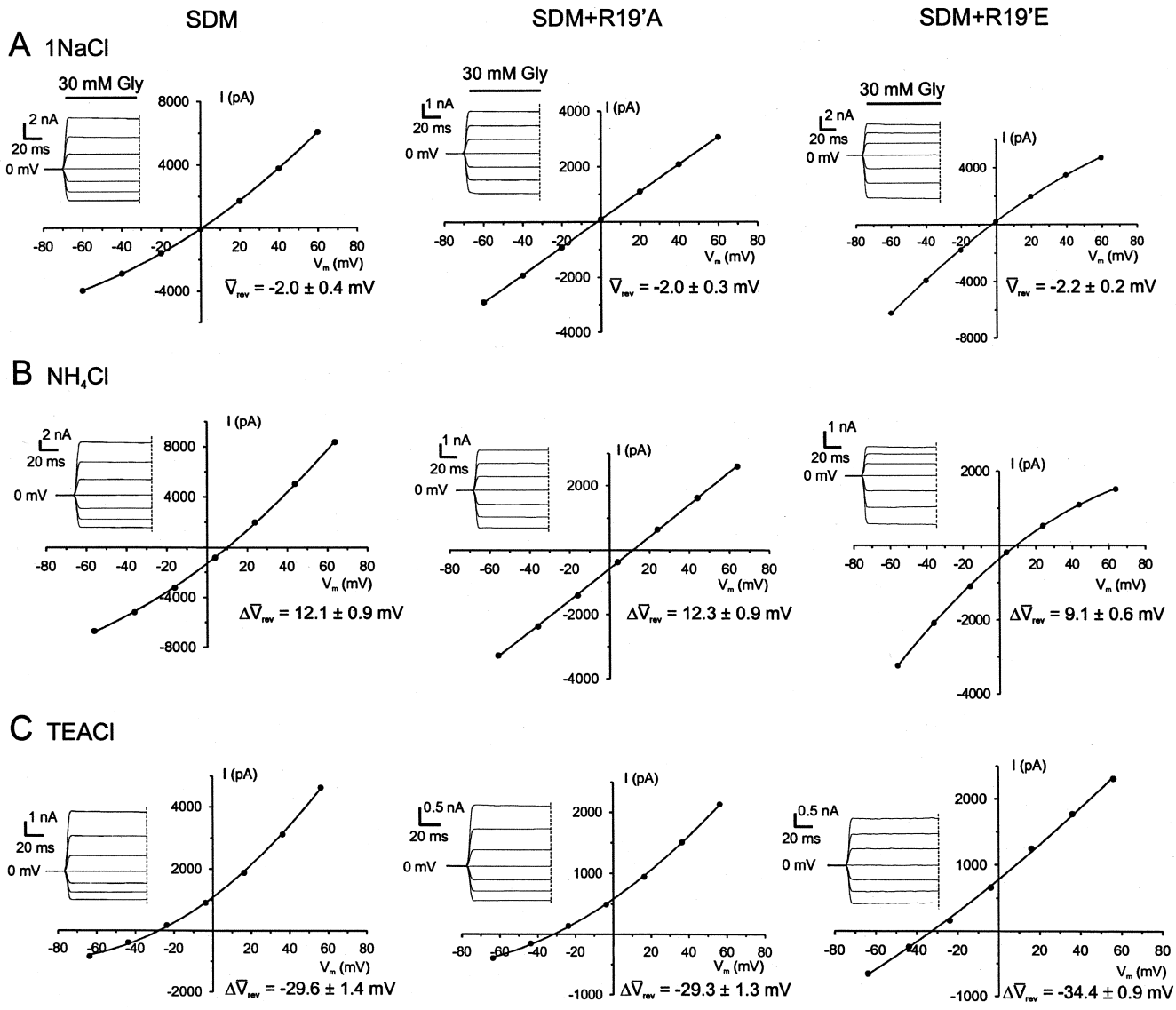

FIGURE 7. Sample biionic I-Vs for determining organic cation permeability. I-V plots and accompanying glycine-activated current responses for experiments to determine the relative permeability of organic cations through three cation-selective GlyR mutant channels. Each column of I-Vs was recorded from the same cell for each mutant GlyR. (A) The control solution was the 1NaCl solution described in the legend to Fig. 4. (B) When NH_4Cl replaced the extracellular NaCl the reversal potential shift (ΔV_{rev}) was to the right (NH_4^+ more permeable than Na^+). (C) When TEACl solution replaced the extracellular NaCl the reversal potential shift was to the left (TEA^+ less permeable than Na^+). Also shown are the average reversal potentials ($\Delta \bar{v}_{rev}$) for SDM ($n = 8$), SDM+R19'A ($n = 9$), and SDM+R19'E ($n = 7$).

GlyR mutants has altered local pore geometry in the opposite direction to that suggested for the α7 nAChR mutations. We speculate that the deletion of the proline residue (P-2'Δ) has produced a conformational twist in the pore constriction region, at least when the channel is in the conducting state. This local geometrical twist may expose the substituted glutamates (A-1'E) to permeating ions, while concomitantly shielding the adjacent R0' residues in the SDM GlyR. This would, in turn, provide a suitable electrical potential and geometric environment favoring the transit of cations. The two single point mutant channels, (A-1'E GlyRs or P-2'Δ GlyRs) each caused profound alterations to the charge selectivity and have added extra information regarding the control of charge selectivity. In particular, the A-1'E mutation by itself produced predominantly cation-selective channels, implying that the introduced negatively charged glutamate prevails electrostatically over the adjacent positively charged arginine (R0'), which confirms the relevance of electrostatics in charge selectivity. The P-2'Δ by itself reduced anion selectivity to render the channels only mildly anion-selective, thus suggesting that pore geometry, in addition to electrostatics, are factors determining charge selectivity.

TABLE II

Permeability Ratios for Organic Cations

Cation	Cation dimensions	Cation mean diameter	A-1'E P_X/P_{Na} (*n*)	SDM P_X/P_{Na} (*n*)	SDM+R19'A P_X/P_{Na} (*n*)	SDM+R19'E P_X/P_{Na} (*n*)
	nm	*nm*				
NH_4^+	0.33 × 0.32 × 0.34	0.33		1.71 ± 0.07 (8)	1.79 ± 0.08 (9)	1.53 ± 0.04 (7)
$TriMA^+$	0.40 × 0.54 × 0.60	0.51	0.43 ± 0.03 (4)	0.85 ± 0.03 (8)	0.62 ± 0.02 (7)	0.57 ± 0.02 (9)
$Tris^+$	0.55 × 0.56 × 0.64	0.58		0.59 ± 0.02 (9)	0.37 ± 0.03 (8)	0.42 ± 0.03 (8)
TMA^+	0.55 × 0.55 × 0.55	0.55	0.06 ± 0.02 (7)	0.56 ± 0.03 (7)	0.31 ± 0.03 (8)	0.29 ± 0.04 (7)
TEA^+	0.58 × 0.70 × 0.70	0.66	0 (5)	0.19 ± 0.02 (9)	0.13 ± 0.02 (8)	0.09 ± 0.02 (7)
TPA^+	0.45 × 1.07 × 1.07	0.86		0.11 ± 0.02 (5)	0 (5)	0 (5)

Permeability ratios relative to sodium (P_X/P_{Na}), were determined from biionic potential experiments for a series of organic cations. The dimensions of the cations were taken from Villarroel et al. (1995) and Kuner et al. (2001). Permeability ratios are stated as mean ± SEM.

Ion channels, which are structurally dissimilar to LGICs, such as the KcsA K^+ channel (Doyle et al., 1998) and the ClC Cl^- channel (Dutzler et al., 2002), appear to select their respective ions via mechanisms that involve the contribution of partial charges from several sources. Crystal structures of both of these channels suggest that α-helix dipoles, in addition to peptide backbone atoms, contribute significantly to the charge selectivity filters. Polar amino acid side chains at the selectivity filter are also believed to interact favorably with Cl^- ions in the ClC Cl^- channel. The only full charge present in the vicinity of the ClC Cl^- channel selectivity filter is a negatively charged glutamate residue, which is believed to separate two Cl^- ions within the pore. This glutamate residue is also thought to pivot out of the conduction pathway during the tightly coupled gating conduction process (Dutzler et al., 2002). The pore-forming M2 helix dipoles in LGICs, including the cation-selective GlyR mutants, are orientated with their NH_2-terminal (positive) ends near the intracellular constriction, which corresponds with the location of the selectivity filter. The COOH-terminal (negative) ends of the M2 helices are therefore situated at the extracellular end of the pore. As this is the case for all LGIC members, regardless of their ion-charge preference, it strongly suggests that pore helix dipoles in LGICs do not make a significant impact on charge selectivity.

The changes in charge of the extracellular ring of charge from positive (SDM and A-1'E GlyRs) to neutral (SDM+R19'A GlyRs) and then to negative (SDM+R19'E GlyRs) revealed no remarkable changes in P_{Cl}/P_{Na}. In fact, the most cation-selective mutant (SDM, $P_{Cl}/P_{Na} = 0.13$) has positively charged arginines at position 19'. The WT α7 nAChR, which has negatively charged glutamates at the extracellular mouth of the pore (E20', Fig. 1), has a very similar P_{Cl}/P_{Na} value to the SDM GlyR ($P_{Cl}/P_{Na} = 0.1$; Bertrand et al., 1993). The slight decrease in P_{Cl}/P_{Na} observed with the R19' mutations may reflect some subtle compensating allosteric change in pore structure that affects the selectivity filter. Therefore, our results show that the charge at the extracellular mouth of the channel has no significant direct influence on monovalent charge selectivity.

Alkali-Cation Permeability in SDM GlyR Channels

The alkali-cation permeability sequence determined in the SDM GlyRs is a low field strength permeability sequence resembling that of the nAChRs (Adams et al., 1980; Konno et al., 1991). The halide anion permeability sequence for GlyRs and GABARs is also low field strength (Bormann et al., 1987; Fatima-Shad and Barry, 1993; Wotring et al., 1999). Low field strength permeability sequences are characterized by weak interactions between permeating ions and those pore residues that form interaction site(s). The primary determinant for ion permeation is the relative attraction of ions to pore residues compared with their attraction to water (Eisenman and Horn, 1983) and hence, in these circumstances, the dominant energy component (for ions of the same sign) governing ion permeation is the hydration energy of the ion. Ions with larger crystal radii have lower hydration energies and therefore permeate more readily. The low field strength alkali cation sequence in the cation-selective GlyR, SDM, and the STM (Keramidas et al., 2000) suggest that the mutations to the pore constriction, which convert ion-charge selectivity of the GlyR channel, retain this fundamental permeation property.

Electrostatics at the Selectivity Filter

As an ion traverses the channel pore, having to strip off some of its hydration shell in a region of low dielectric would be expected to impede the motion of the ion as it nears the pore constriction, resulting in steep energy barriers for the permeating ions. In the presence of fixed negative charges (eg., −1'E), the potential at the constriction should provide an energy minimum for cations, while increasing the energy required for anions to pass beyond the constriction. The depth of the energy well for cations would be accentuated by the lower dielectric constant within the channel pore, while the corresponding potential energy required for

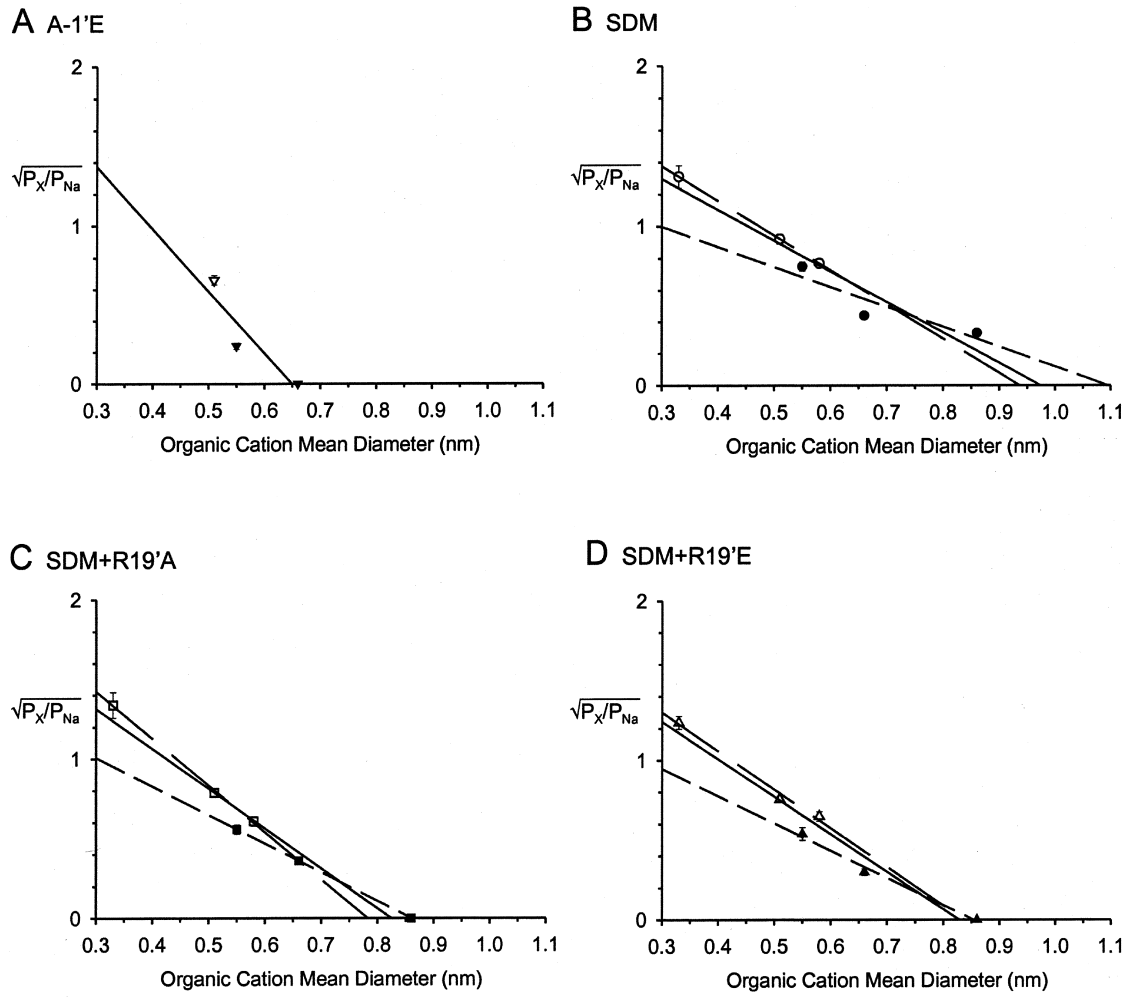

FIGURE 8. Estimates of minimum pore diameters. Plots of the square root of the permeability ratio for four cation-selective GlyR mutants versus organic cation mean diameter. The organic cations tested were: NH_4^+, $TriMA^+$, $Tris^+$, TMA^+, TEA^+, and TPA^+. The data points were fitted to linear regressions and extrapolated to the x-axis to determine minimum pore diameter according to Eq. 5. The organic cations that can form hydrogen bonds (NH_4^+, $TriMA^+$, and $Tris^+$) are shown with open symbols and are fitted with long dashed lines, whereas those that do not form hydrogen bonds (TMA^+, TEA^+, TPA^+) are shown with closed symbols and are fitted with short dashed lines for the SDM-based GlyRs. The solid line fit is the average fit to all the data points. The values for the minimum diameter of the pore (using the data from all the cations) for A-1'E (A, ▼) is 0.65 nm, SDM (B, ●) is 0.97 nm, SDM+R19'A (C, ■) is 0.82 nm, and SDM+R19'E (D, ▲) is 0.83 nm.

anion permeation would increase (Kuyucak et al., 1998). An applied membrane potential would intensify the intrinsic electric field of the open channel at the pore constriction, as demonstrated experimentally by Pascual and Karlin (1998) for the muscle nAChR channel. For the open nAChR channel, this negative intrinsic electrostatic potential has been shown to arise primarily due to the ring of E-1' residues and decreases in magnitude linearly as the total charge at this intermediate ring is reduced (Wilson et al., 2000). Therefore, to a large extent, the P_{Cl}/P_{Na} values obtained in our experiments could be explained qualitatively in terms of permeating ion and −1'E side chain interactions. For cations, the pore constriction would provide an energy well, which would be lower than that for anions. The smaller proportion of Cl^- ions with sufficient kinetic energy to traverse the pore constriction would then result in a lower relative anion permeability. Notably, the cation selectivity of the single GlyR mutant (A-1'E) strongly implies that the electronegative environment required for cation conduction is provided by the negatively charged side chains of the introduced glutamate residues. This inference is in contrast to the conclusion favored by Corringer et al. (1999) and concurred by Gunthorpe and Lummis (2001) for the α7 nAChR and 5-HT_{3A}R, respectively, in which it was suggested that the peptide backbone contributes to a suitable electrostatic environment at the selectivity filter. The key anion-selective α7 nAChR mutant channel that led Corringer et al. (1999) to infer this included the substitution of

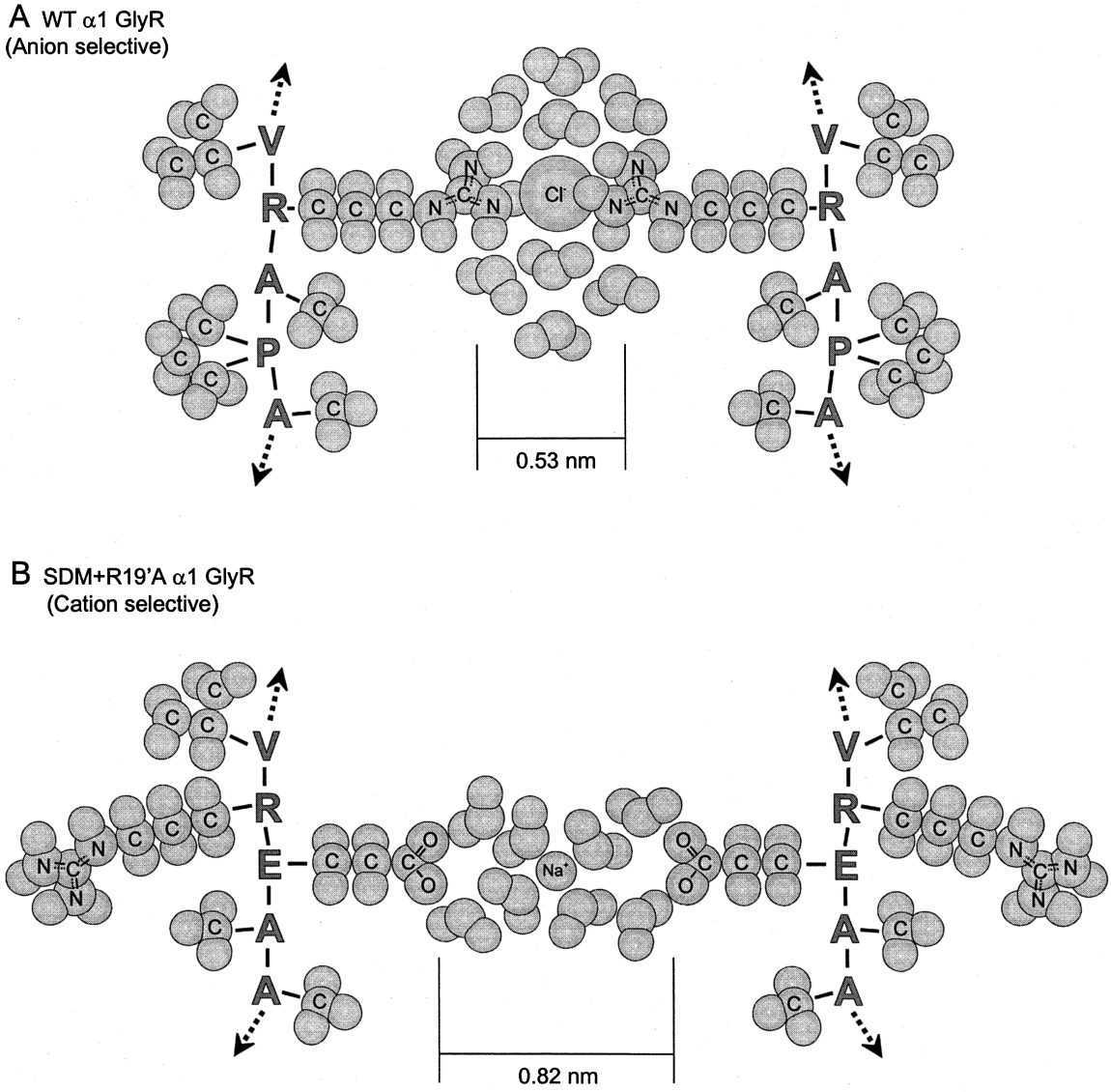

FIGURE 9. Schematic representation of the selectivity filter. A hypothetical representation of two M2 domains in the region of the selectivity filter between positions 1' to −3' or −4'. Atoms and ions are drawn as spheres and to approximate scale. For simplicity, only the side chains of the amino acid residues are shown, the remainder of the residues (peptide backbone) are represented by the single letter code for the amino acids. (A) The anion-selective WT α1 GlyR with a partially hydrated Cl^- ion closely interacting with the positively charged side chains of arginine residues (R0'). (B) The cation-selective SDM+R19'A α1 GlyR with a more hydrated Na^+ ion interacting with the side chains of introduced negatively charged glutamate residues (−1'E).

the positively charged lysine with glutamine at position 0' in addition to a number of other M2 mutations. As this multiple α7 nAChR mutant also includes the −2'P insertion (and the E-1'A), our model would suggest that the introduced glutamine (K0'Q) would be exposed to permeating ions. In addition, since glutamine is a polar molecule, it seems possible that the positive end of its dipole could be contributing to an electrostatic environment favorable to anions. Furthermore, our data indicates that pore size can also influence charge selectivity and it is unclear how the nAChR mutations alter pore diameter.

Diameter of the Selectivity Filter

It has been shown that within the LGIC family, the cation-selective channels are consistently larger than their anion-selective counterparts. Typically, the diameters of nAChRs and 5-HT_3Rs range between 0.74 and 0.84 nm (Dwyer et al., 1980; Yang, 1990; Cohen et al., 1992a), whereas the diameters of anion-selective GlyRs and GABARs are typically in the range of ∼0.5–0.6 nm (Bormann et al., 1987; Fatima-Shad and Barry, 1993; Rundstrom et al., 1994; Wotring et al., 1999). Our experiments show that there is a concomitant enlargement of

the narrow selectivity filter accompanying the reversal in ion charge selectivity from anion- to cation-selective in the four GlyR mutants tested. These four GlyRs, A-1'E, SDM, SDM+R19'A, and SDM+R19'E, have minimum pore diameters of 0.65, 0.97, 0.82, and 0.83 nm, respectively, all of which are larger than the WT α1 GlyR (0.53 nm; Rundstrom et al., 1994). The A-1'E GlyR, which is the least cation permeable has a diameter that is most similar to the WT. The SDM-based GlyRs have pore diameters, which are more comparable to those of the cation-selective nAChRs. Further, it is likely that the mutation contributing most to the widening of the selectivity filter is the proline deletion at −2'.

Data from all LGICs tested so far, including the cation-selective GlyRs, the STM (Keramidas et al., 2000), and the SDM, imply low field strength interactions between ions and pore-lining residues, a phenomenon where permeation is dominated by ion hydration. It therefore seems reasonable to correlate minimum pore diameter with the size of partially hydrated ions. The available data corroborate a permeation model where the larger pores of the cation-selective GlyR mutants facilitate the more heavily hydrated Na^+ ions, allowing them to transit the selectivity filter completely surrounded by water molecules (Fig. 9 B). In contrast, the more easily dehydrated Cl^- ions require closer interactions with the charged residues of the selectivity filter (Fig. 9 A). In both cases, the diameter of the selectivity filter sets constraints on how easily the charged residues of the selectivity filter can compensate adequately for the hydration energy of the ions. A similar "precise fit" hypothesis has been advanced to explain the high selectivity for K^+ ions in the KcsA K^+ channel (Doyle et al., 1998).

It should be born in mind that the approach of using permeant ions of increasing size to determine the dimensions of the channel pore has some inherent simplifications. The model assumes that ions in the channel do not interact electrostatically with each other or with the wall of the channel and that ions permeate by a size sieving effect. It also assumes that the channel wall and the permeating ions are featureless.

Using organic cations of different chemical natures can provide information regarding the orientation of residues lining the channel wall. Of the organic cations used in this study, three are capable of forming hydrogen bonds, NH_4^+, $TriMA^+$, and $Tris^+$, with $Tris^+$ contributing two groups for hydrogen bonding, whereas the three fully methylated cations (TMA^+, TEA^+, and TPA^+) do not form hydrogen bonds. It has been noted that cations with hydrogen bonding donor groups (−OH or −NH) can appear smaller when interacting with hydrogen bond acceptors (−O). That is, the donor and acceptor can approach each other closer than their van der Waals dimensions, by ∼0.09 nm (e.g., Hille, 1971). For all mutant GlyRs tested, $Tris^+$ was more permeant than TMA^+ even though it is a larger ion (Table II). When the hydrogen-bonding organic cations were fitted separately, as illustrated in Fig. 8 for each mutant tested, the fits yielded noticeably smaller minimum pore diameters for two of the GlyRs, the SDM and SDM+R19'A (0.93 and 0.78 nm, respectively). Conversely, when the nonhydrogen-bonding organic cations were fitted separately the fits gave larger pore diameter estimates for the SDM and SDM+R19'A (1.1 and 0.86 nm, respectively). These results imply that, for at least two of the GlyR mutants, the channel walls are lined with polar residues (threonines and serines, see Fig. 1), which provide hydrogen bond acceptors.

Ca^{2+} Permeability in SDM-Based GlyR Channels.

The three cation-selective mutant GlyRs tested for Ca^{2+} permeability were all able to pass Ca^{2+} ions. The SDM GlyR allows a significant Ca^{2+} permeability with $P_{Ca}/P_{Na} = 0.29$, which is higher than the value reported for the amphibian skeletal muscle nAChRs ($P_{Ca}/P_{Na} = 0.16$; Adams et al., 1980). Galzi et al. (1992) reported that neutralizing the intermediate ring in the α7 nAChR (E-1'A) produced channels that were permeant to monovalent cations but had lost their ability to allow Ca^{2+} ions to permeate. This result suggested that the presence of the appropriate charge in the intermediate ring is essential for divalent charge discrimination.

The cation-selective GlyR (STM; P-2'Δ, A-1'E, and T13'V), reported previously by Keramidas et al. (2000), displayed no Ca^{2+} permeability despite having the P-2'Δ, A-1'E mutations at the intermediate ring. The SDM GlyR retains a threonine at position 13' and is permeable to Ca^{2+}, an observation which is consistent with the increase in Ca^{2+} permeability seen in the α7 nAChR mutant, V13'T, compared with the WT α7 nAChR (Bertrand et al., 1993). We infer that the valine residue at position 13' in the STM GlyR serves to attenuate Ca^{2+} permeability, whereas favorable ionic interactions occur with the polar threonine in the SDM GlyR, resulting in an enhancement of Ca^{2+} permeability. Our other two cation-selective mutant GlyRs have even higher relative P_{Ca}/P_{Na} values, comparable to those of nAChRs reported in parasympathetic cardiac neurons ($P_{Ca}/P_{Na} = 0.93$; Fieber and Adams, 1991) and the homomeric 5-HT_{3A}R ($P_{Ca}/P_{Na} = 1.0$; Brown et al., 1998). In addition, there was no strong correlation between P_{Cl}/P_{Na} and P_{Ca}/P_{Na} values for the three cation-selective GlyRs (Table I). These observations strongly suggest that, in addition to the charge-selective pore constriction and the presence of T13' in all the mutants in this paper, Ca^{2+} ion permeation is strongly influenced by the appropriate charge in the extracellular ring. The SDM+R19'A and SDM+R19'E channels present extracellular vestibules with a nonrepulsive net charge, in contrast to the SDM GlyR, which has five positively charged resi-

dues at the extracellular channel entrance (R19'). Neutralization of this charge occurs with the SDM+R19'A GlyR (R19'A) and the charge at the extracellular mouth of the channel becomes negative in the SDM+R19'E (R19'E) GlyR. Note that all three mutants have negatively charged intermediate and cytoplasmic rings (Fig. 1). Therefore, the increase in Ca^{2+} permeability seen in the SDM+R19'A and SDM+R19'E can, in part, be attributed to the charge at the extracellular ring (see also Dani, 1986), as also suggested by the progressive increase in inward Ca^{2+} current relative to outward Na^+ current from SDM to SDM+R19'A and then to SDM+R19'E (Fig. 6 B). The cation-selective GlyR mutants, however, did not attain the permeability of the WT α7 nAChR (P_{Ca}/P_{Na} = 10; Bertrand et al., 1993). At positions 16' and 17' the α7 nAChR has nonpolar leucine residues (L16' and L17', Fig. 1). Mutating either of these leucines to nonconservative residues such as glycine, threonine, glutamine, and arginine in the α7 nAChR drastically reduced or abolished Ca^{2+} permeability (Bertrand et al., 1993). In the GlyR, serine and glycine (S16' and G17') occupy these positions. Hence, our results are consistent with those of Bertrand et al. (1993) for the α7 nAChR, which indicate that nonconservative substitutions at positions 16' and 17' attenuates Ca^{2+} permeability. It should be noted, however, that our study, and especially that of Bertrand et al. (1993), indicates that Ca^{2+} permeability may also be facilitated by other sites within the M2 domains of LGICs.

Conclusion

The present study elucidates several key determinants of ion-charge selectivity in α1 homomeric GlyRs. We have shown that a single point mutation (A-1'E) at the intracellular end of the M2 domain is sufficient to convert the anion-selective GlyR to selectively pass cations. This result demonstrates the importance of an appropriate electrostatic environment at the pore constriction contributed by amino acid side chains and isolates the region of the selectivity filter with fine resolution. The results also reveal that the diameter of the selectivity filter is a significant factor in ion charge discrimination with larger minimum pore diameters facilitating cation permeation. Furthermore, the permeability of calcium ions is shown to also depend on the charged M2 residues at the extracellular mouth of the pore. It seems reasonable that calcium, being a divalent ion, is especially sensitive to the electrostatic environment of the pore vestibule, and increases its permeability when the positive charge (R19') of the extracellular mouth of the pore is neutralized or made negative. The ability to convert GlyRs into calcium conducting channels may facilitate a complementary method of investigating GlyR function by using calcium-imaging techniques.

We thank Irene Michas and Anna Heath for preparing the cell cultures and transfections and Dr. Anna C. Park for help with some experiments. We also thank Dr. Trevor Lewis for critical reading of the manuscript.

The National Health and Medical Research Council of Australia (project grant 9935846 and block grant 993050), a 2002 University Research Support Program Grant (URSP), and the Australian Research Council supported this work.

Submitted: 27 December 2001
Revised: 22 March 2002
Accepted: 22 March 2002

REFERENCES

Adams, D.J., T.M. Dwyer, and B. Hille. 1980. The permeability of endplate channels to monovalent and divalent metal cations. *J. Gen. Physiol.* 75:493–510.

Barry, P.H. 1994. JPCalc, a software package for calculating liquid junction potential corrections in patch-clamp, intracellular, epithelial and bilayer measurements and for correcting junction potential measurements. *J. Neurosci. Methods.* 51:107–116.

Barry, P.H., and P.W. Gage. 1984. Ionic selectivity of channels at the end plate. *Current Topics in Membranes and Transport.* 21:1–51.

Bertrand, D., J.L. Galzi, A. Devillers-Thiéry, S. Bertrand, and J.P. Changeux. 1993. Mutations at two distinct sites within the channel domain M2 alter calcium permeability of neuronal α7 nicotinic receptor. *Proc. Natl. Acad. Sci. USA.* 90:6971–6975.

Bormann, J., O.P. Hamill, and B. Sakmann. 1987. Mechanism of anion permeation through channels gated by glycine and γ-aminobutyric acid in mouse cultured spinal neurons. *J. Physiol.* 385: 243–286.

Brown, A.M., A.G. Hope, J.J. Lambert, and J.A. Peters. 1998. Ion permeation and conduction in the human recombinant 5-HT_3 receptor subunit (h5-HT_{3A}). *J. Physiol.* 507:653–665.

Chen, C., and H. Okayama. 1987. High efficiency expression of mammalian cells by plasmid DNA. *Mol. Cell. Biol.* 7:2745–2751.

Cohen, B.N., C. Labarca, L. Czyzyk, N. Davidson, and H.A. Lester. 1992a. Mutations in M2 alter the selectivity of the mouse nicotinic acetylcholine receptor for organic and alkali metal cations. *J. Gen. Physiol.* 100:373–400.

Cohen, B.N., C. Labarca, L. Czyzyk, N. Davidson, and H.A. Lester. 1992b. Tris+/Na+ permeability ratios of nicotinic acetylcholine receptors are reduced by mutations near the intracellular end of the M2 region. *J. Gen. Physiol.* 99:545–572.

Corringer, P.J., S. Bertrand, J.L. Galzi, A. Devillers-Thiéry, J.P. Changeux, and D. Bertrand. 1999. Mutational analysis of the charge selectivity filter of the α7 nicotinic acetylcholine receptor. *Neuron.* 22:831–843.

Couturier, S., D. Bertrand, J.-M. Matter, M.-C. Hernandez, S. Bertrand, N. Millar, S. Valera, T. Barkas, and M. Ballivet. 1990. A neuronal nicotinic acetylcholine receptor subunit (α7) is developmentally regulated and forms a homo-oligomeric channel blocked by α-BTX. *Neuron.* 5:847–856.

Dani, J.A. 1986. Ion-channel entrances influence permeation. *Biophys. J.* 49:607–618.

Doyle, D.A., J.M. Cabral, R.A. Pfuetzner, A. Kou, J.M. Gublis, L. Cohen, B.T. Chait, and R. MacKinnon. 1998. The structure of the potassium channel: molecular basis of K^+ conduction and selectivity. *Science.* 280:69–77.

Dutzler, R., E.B. Campbell, M. Cadene, B.T. Chait, and R. MacKinnon. 2002. X-Ray structure of a ClC channel at 3.0Å reveals the molecular basis of anion selectivity. *Nature.* 415:287–294.

Dwyer, T.M., D.J. Adams, and B. Hille. 1980. The permeability of the endplate channel to organic cations in frog muscle. *J. Gen. Physiol.* 75:469–492.

Eisenman, G., and R. Horn. 1983. Ionic selectivity revisited: the role of kinetic and equilibrium processes in ion permeation through channels. *J. Membr. Biol.* 76:197–225.

Fatima-Shad, K., and P.H. Barry. 1993. Anion permeation in GABA and glycine-gated channels of mammalian cultured hippocampal neurons. *Proc. R. Soc. Lond. B. Biol. Sci.* 253:69–75.

Fieber, L.A., and D.J. Adams. 1991. Acetylcholine-evoked currents in cultured neurones dissociated from rat parasympathetic cardiac ganglia. *J. Physiol.* 434:215–237.

Galzi, J.L., A. Devillers-Thiéry, N. Hussey, S. Bertrand, J.P. Changeux, and D. Bertrand. 1992. Mutations in the channel domain of a neuronal nicotinic receptor convert ion selectivity from cationic to anionic. *Nature.* 359:500–505.

Grenningloh, G., A. Rienitz, B. Schmitt, C. Methfessel, M. Zensen, K. Beyreuther, E.D. Gundelfinger, and H. Betz. 1987. The strychnine-binding subunit of the glycine receptor shows homology with nicotinic acetylcholine receptors. *Nature.* 328:215–220.

Gunthorpe, M.J., E.J. Fletcher, and S.C.R. Lummis. 1996. Conversion of the ion selectivity of the 5-HT_3 receptor from cationic to anionic: a conserved feature of the ligand gated ion channel superfamily? *Br. J. Pharmacol.* 119:259P.

Gunthorpe, M.J., and S.C.R. Lummis. 2001. Conversion of the ion selectivity of the 5-HT_{3A} receptor from cationic to anionic reveals a conserved feature of the ligand-gated ion channel superfamily. *J. Biol. Chem.* 276:10977–10983.

Hille, B. 1971. The permeability of the sodium channel to organic cations in myelinated nerve. *J. Gen. Physiol.* 58:599–619.

Ho, S.N., D.H. Hunt, R.M. Horton, J.K. Pullen, and L.R. Pease. 1989. Site-directed mutagenesis by overlap extension using the polymerase chain reaction. *Gene.* 77:51–59.

Imoto, K., C. Busch, B. Sakmann, M. Mishina, T. Konno, J. Nakai, H. Bujo, Y. Mori, K. Fukuda, and S. Numa. 1988. Rings of negatively charged amino acids determine the acetylcholine receptor channel conductance. *Nature.* 335:645–648.

Karlin, A., and M.H. Akabas. 1995. Towards a structural basis for the function of nicotinic acetylcholine receptors and their cousins. *Neuron.* 15:1231–1244.

Keramidas, A., A.J Moorhouse, C.R French, P.R Schofield, and P.H Barry. 2000. M2 pore mutations convert the glycine receptor channel from being anion- to cation-selective. *Biophys. J.* 78:247–259.

Konno, T., C. Busch, E. Von Kitzing, K. Imoto, F. Wang, J. Nakai, M. Mishina, S. Numa, and B Sakmann. 1991. Rings of anionic amino acids as structural determinants of ion selectivity in the acetylcholine receptor channel. *Proc. R. Soc. Lond. B. Biol. Sci.* 244:69–79.

Kuner, T., C. Beck, B. Sakmann, and P.H. Seeburg. 2001. Channel-lining residues of the AMPA receptor M2 segment: structural environment of the Q/R Site and identification of the selectivity filter. *J. Neurosci.* 21:4162–4172.

Kuyucak, S., M. Hoyles, and S.-H. Chung. 1998. Analytical solutions of poisson's equations for realistic geometrical shapes of membrane ion channels. *Biophys. J.* 74:22–36.

Langosch, D., L. Thomas, and H. Betz. 1988. Conserved quaternary structure of ligand-gated ion channels: the post synaptic glycine receptor is a pentamer. *Proc. Natl. Acad. Sci. USA.* 85:7394–7398.

Langosch, D., B. Laube, N. Rundstrom, V. Schmieden, J. Bormann, and H. Betz. 1994. Decreased agonist affinity and chloride conductance of mutant glycine receptors associated with human hereditary hyperekplexia. *EMBO J.* 13:4223–4228.

Le Novère, N., and J.-P. Changeux. 1999. The ligand gated ion channel database. *Nucleic Acid Res.* 27:340–342.

Lester, H.A. 1992. The permeation pathway of neurotransmitter-gated ion channels. *Annu. Rev. Biophys. Biomol. Struct.* 21:267–292.

Maricq, A.V., A.S. Peterson, A.J. Brake, R.M. Myers, and D. Julius. 1991. Primary structure and functional expression of the $5HT_3$ receptor, a serotonin-gated ion channel. *Science.* 254:432–437.

Moorhouse, A.J., A. Keramidas, A. Zaykin, P.R. Schofield, and P.H. Barry. 2002. Single channel analysis of conductance and rectification in cation-selective, mutant glycine receptor-channels. *J. Gen Physiol.* 119:411–425.

Noda, M., H. Takahashi, T. Tanabe, M. Toyosato, S. Kikyotani, Y. Furutani, T. Hirose, H. Takashima, S. Inayama, T. Miyata, and S. Numa. 1983. Structural homology of *Torpedo californica* acetylcholine receptor subunits. *Nature.* 302:528–532.

Pascual, J.M., and A. Karlin. 1998. State-dependent accessibility and electrostatic potential in the channel of the acetylcholine receptor. *J. Gen. Physiol.* 111:717–739.

Rajendra, S., J.W. Lynch, K.D. Pierce, C.R. French, P.H. Barry, and P.R. Schofield. 1994. Startle disease mutations reduce the agonist sensitivity of the human inhibitory glycine receptor. *J. Biol. Chem.* 269:18739–18742.

Rajendra, S., J.W. Lynch, K.D. Pierce, C.R. French, P.H. Barry, and P.R. Schofield. 1995. Mutation of an arginine residue in the human glycine receptor transforms β-alanine and taurine from agonists to competitive antagonists. *Neuron.* 14:169–175.

Reeves, D.C., E.N. Goren, M.H. Akabas, and S.C.R. Lummis. 2001. Structural and electrostatic properties of the 5-HT_3 receptor pore revealed by substituted cysteine accessibility mutagenesis. *J. Biol. Chem.* 276:42035–42042.

Robinson, R.A., and R.H. Stokes. 1965. Electrolyte Solutions. 2nd Ed. Butterworths, London. 571 pp.

Rundstrom, N., V. Schmieden, H. Betz, J. Bormann, and D. Langosch. 1994. Cyanotriphenylborate: subtype-specific blocker of glycine receptor chloride channels. *Proc. Natl. Acad. Sci. USA.* 91: 8950–8954.

Saul, B., T. Kuner, D. Sobetzko, W. Brune, F. Hanefeld, H.M. Meinck, and C.M. Becker. 1999. Novel GLRA1 missense mutation (P250T) in dominant hyperekplexia defines an intracellular determinant of glycine receptor channel gating. *J. Neurosci.* 19: 869–877.

Schofield, P.R., M.G. Darlison, N. Fujita, D.R. Burt, F.A. Stephenson, H. Rodriguez, L.M. Rhee, J. Ramachandran, V. Reale, T.A. Glencorse, et al. 1987. Sequence and functional expression of the $GABA_A$ receptor shows a ligand-gated receptor superfamily. *Nature.* 328:221–227.

Villarroel, A., N. Burnashev, and B. Sakmann. 1995. Dimensions of the narrow portion of a recombinant NMDA receptor channel. *Biophys. J.* 68:866–875.

Wang, F., and K. Imoto. 1992. Pore size and negative charge as structural determinants of permeability in the *Torpedo* nicotinic acetylcholine receptor channel. *Proc. R. Soc. Lond. B. Biol. Sci.* 250:11–17.

Wotring, V.E., C. Yongchang, and D.S. Weiss. 1999. Permeability and single channel conductance of human homomeric ρ1 $GABA_C$ receptors. *J. Physiol.* 521:327–336.

Wilson, G.G., and A. Karlin. 1998. The location of the gate in the acetylcholine receptor channel. *Neuron.* 20:1269–1281.

Wilson, G.G., and A. Karlin. 2000. Acetylcholine receptor channel structure in the resting, open, and desensitized states probed with the substituted-cysteine-accessibility method. *Proc. Natl. Acad. Sci. USA.* 98:1241–1248.

Wilson, G.G., P.M. Pascual, N. Brooijmans, D. Murray, and A. Karlin. 2000. The intrinsic electrostatic potential and the intermediate ring of charge in the acetylcholine receptor channel. *J. Gen. Physiol.* 115:93–106.

Xu, M., and M.H. Akabas. 1996. Identification of channel-lining residues in the M2 membrane-spanning segment of the $GABA_A$ receptor α_1 subunit. *J. Gen. Physiol.* 107:195–205.

Yang, J. 1990. Ion permeation through 5-hydroxytryptamine–gated channels in neuroblastoma N18 cells. *J. Gen. Physiol.* 96:1177–1198.